The role of climate change in extreme rainfall associated with Cyclone Gabrielle over Aotearoa New Zealand's East Coast

Luke J. Harrington[1], Sam M. Dean[2], Shaun Awatere[3,4], Suzanne Rosier[2], Laura Queen[2], Peter B. Gibson[2], Clair Barnes[5], Mariam Zachariah[5], Sjoukje Philip[6], Sarah Kew[6], Gerbrand Koren[7], Izidine Pinto[6], Matthew Grieco[8], Maja Vahlberg[9], Roop Singh[9], Dorothy Heinrich[9], Lisa Thalheimer[10], Sihan Li[11], Dáithí Stone[2], Wenchang Yang[12], Gabriel A. Vecchi[12,13], David J. Frame[14], Friederike E.L. Otto[6]

1. Te Aka Mātuatua School of Science, Te Whare Wānanga o Waikato/University of Waikato, Kirikiriroa/Hamilton 3216, Aotearoa New Zealand
2. Taihoro Nukurangi/National Institute of Water and Atmospheric Research (NIWA), Hataitai, Pōneke/Wellington 6021, Aotearoa New Zealand
3. Manaaki Whenua - Landcare Research, Hillcrest, Kirikiriroa/Hamilton 3216, Aotearoa New Zealand
4. Ngā Pae o te Māramatanga, Waipapa Taumata Rau/University of Auckland, Tāmaki Makaurau/Auckland 1142, Aotearoa New Zealand
5. Grantham Institute, Imperial College London, UK
6. Royal Netherlands Meteorological Institute (KNMI), De Bilt, The Netherlands
7. Copernicus Institute of Sustainable Development, Utrecht University, Utrecht, the Netherlands
8. Global Disaster Preparedness Center, American Red Cross, Washington DC, USA
9. Red Cross Red Crescent Climate Centre, The Hague, the Netherlands
10. United Nations University, Institute for Environment and Human Security, Bonn, Germany.
11. Department of Geography, University of Sheffield
12. Department of Geosciences, Princeton University, Princeton, NJ 08544, USA
13. High Meadows Environmental Institute, Princeton University, Princeton, NJ 08544, USA
14. School of Physical and Chemical Sciences, Te Whare Wānanga o Waitaha/University of Canterbury, Ōtautahi/Christchurch 8140, Aotearoa New Zealand.

Glossary for place names

Aotearoa - New Zealand
Te Ika-a-Māui - North Island
Te Tai Tokerau - Northland
Tāmaki Makaurau - Auckland
Te Tairāwhiti - Gisborne
Te Matau-a-Māui - Hawke's Bay
Te Moana-a-Toi - Bay of Plenty
Heretaunga - Hastings
Ahuriri - Napier
Tākawira - Dargaville
Te Tara-O-Te-Ika-A-Māui - Coromandel Peninsula
Ōtautahi - Christchurch

1

Pōneke - Wellington
Kirikiriroa - Hamilton
Waitaha - Canterbury
Te Whare Wānanga o Waikato - University of Waikato
Taihoro Nukurangi - National Institute of Water and Atmospheric Research (NIWA)
Waipapa Taumata Rau - University of Auckland
Te Whare Wānanga o Waitaha - University of Canterbury
Te Ratonga Titirangi - MetService

1. Introduction

Tropical cyclones (TCs) occur regularly in the South Pacific Ocean, with the potential for impacts omnipresent for all countries in the region during the Southern Hemisphere summer. Situated in the lower reaches of the south-west Pacific basin, these risks also extend to Aotearoa New Zealand (ANZ): impactful wind- and rain-related hazards can often occur when ex-Tropical Cyclones pass close to the country, with relative risks highest for north-facing regions of Te Ika-a-Māui (North Island). The official Tropical Cyclone season for the Southwest Pacific basin runs from November to April, with the peak of the season coinciding with the late austral summer months of February and March. In its October 2022 outlook, a combination of regional meteorological services concluded that a 'normal' season of six to ten named TCs was likely for the 2022/23 Tropical Cyclone season, though with elevated TC activity in the Coral Sea and Vanuatu regions in part driven by the continuation of La Niña conditions for a third consecutive summer. The outlook similarly noted that "the risk for an ex-tropical cyclone affecting Aotearoa is considered near normal to elevated" for similar reasons.

In early February 2023, a tropical low pressure system formed in the Pacific Ocean to the north of Fiji before slowly moving westwards into the Coral Sea. A cyclone subsequently formed in the open oceans to the south of the Solomon Islands where, surrounded by sea surface temperatures much warmer than normal (approaching 30°C), both oceanic and atmospheric conditions were favourable for the system to intensify. Tropical Cyclone Gabrielle was officially named by the Australian Bureau of Meteorology on February 8th, strengthening to its peak Category 3 status on February 10th while situated to the north-west of Norfolk Island (figure 1). As was predicted more than a week in advance by ANZ's MetService, the system continued to track south-east towards the northern coastlines of ANZ, transitioning to an extratropical cyclone early in the morning of February 12.
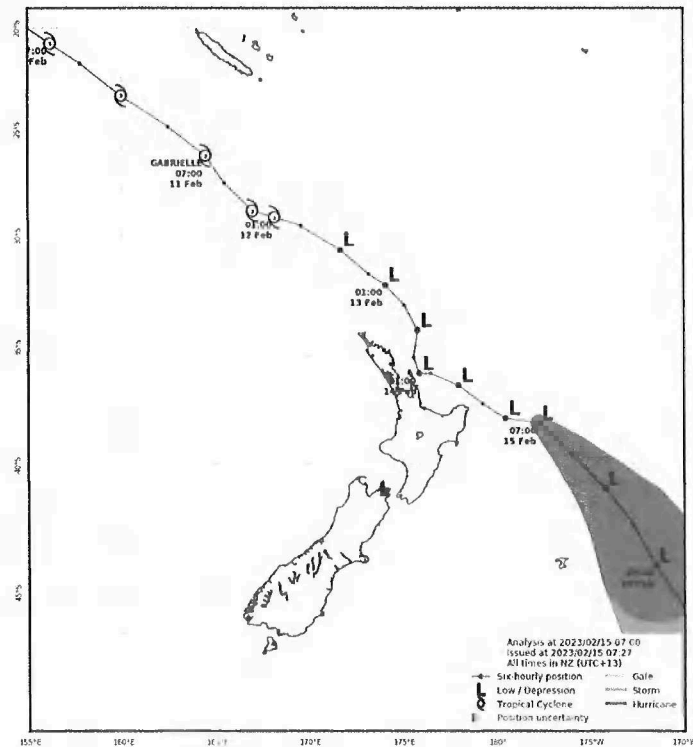
Figure 1: Cyclone Gabrielle track analysis and forecast as of 07:27 February 15 2023. Black circles along the cyclone's track denote six-hourly time steps. Source: MetService.

With heavy rain watches upgraded to orange and then red heavy rain warnings throughout the day of February 11, heavy rain first arrived in Te Tai Tokerau (Northland) andTāmaki Makaurau (Auckland) throughout February 12 as Gabrielle continued its approach from the north-west. The following day, a passing trough from the Tasman Sea provided Cyclone Gabrielle with extra energy while also causing its track to adjust south towards the Te Tara-O-Te-Ika-A-Māui (Coromandel Peninsula) and stall (with a significant high pressure system sitting to the south-east of the country also playing a role in its slow passage). By midnight of February 13, the centre of Gabrielle was situated over Great Barrier Island, during which time mean sea level pressure was recorded at 966.6hPa nearby. Over the following two days, the centre of Cyclone Gabrielle slowly passed eastwards above the northern coastlines of the Bay of Plenty (Te Moana-a-Toi) and Te Tairāwhiti regions before its influence over the country finally began to wane by February 15.

1.1 Summary of impacts

As the centre of the system stagnated to the east of Te Tara-O-Te-Ika-A-Māui, the night of February 13/14 marked the most intense passage of rainfall associated with Cyclone Gabrielle for many regions, particularly Te Tairāwhiti (Gisborne) and Te Matau-a-Māui (Hawke's Bay). Rainfall rates exceeded 20 mm/hour for more than six hours across multiple high-elevation rain gauges in these regions, with the headwaters of the Maunganui (Esk Valley) and Wairoa regions of northern Te Matau-a-Māui witnessing particularly severe rainfall anomalies (figure 2).

3
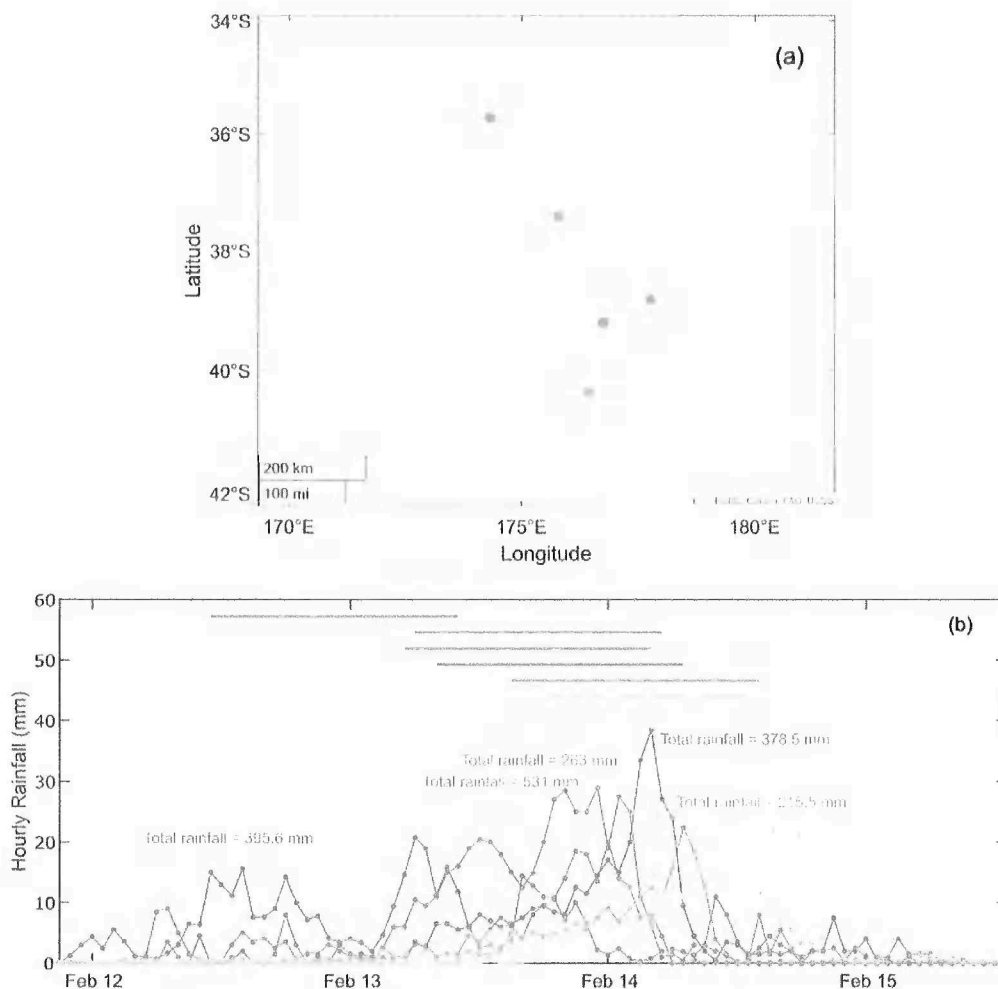
Figure 2: Hourly rainfall accumulations from selected weather stations across the northern and eastern coastlines of Te Ika-a-Māui. Coloured horizontal bars in panel b denote timing of peak 24-hour period of rainfall at each station. Stations chosen - listed in order from north to south - are as follows: (1) Whangārei (Waiarohia at NRC Water St); (2) Te Tara-O-Te-Ika-A-Māui (Ohinemuri River - Queens Head); (3) Te Tairāwhiti (Fairview); (4) Esk Valley (Maunganui); (5) Tararua (Mangaorapa); Wairarapa (Te Wharau).

However, the impacts of heavy rain were throughout the northern and eastern coastlines of the Te Ika-a-Māui - this large footprint of impacts arguably one of the defining features of this event (MetService, 2023). Among examples from other regions, between 250 - 400mm of rain was recorded across Te Tai Tokerau region, with flooding reported in the town of Tākawira (Dargaville) and Whangārei Airport receiving 320 mm of rain across the duration of the event. Parts of the Tāmaki Makaurau region recorded more than 200 mm of rain, including Waitakere (248 mm). Multiple roads were impacted by slips in Te Tara-O-Te-Ika-A-Māui and flooding was also recorded in the Hauraki district. Further to the south, stations in both the Tararua and Wairarapa districts recorded their highest rainfall in several years, with residents in the Pohangina Valley also cut off due to flooding impacts.

Other hazards associated with the cyclone further compounded regional impacts. Storm surges of more than 0.5m brought extreme coastal erosion and flooding along the eastern seaboards of both Te Tai Tokerau and Te Tara-O-Te-Ika-A-Māui (Whitianga recorded surges of at least 0.7m and experienced widespread coastal flooding during local high tides). Later on the 13th and 14th of February, strong wind gusts were recorded across the Central Te Ika-a-Māui, Taranaki and particularly Tāmaki Makaurauand Te Tai Tokerau - one weather station in Te Tai Tokerau (Tākawira) recorded wind gusts

4

of 127 km/hr, for example (see figure 3). These high winds combined with saturated land from previous rains to cause multiple power outages across the region.
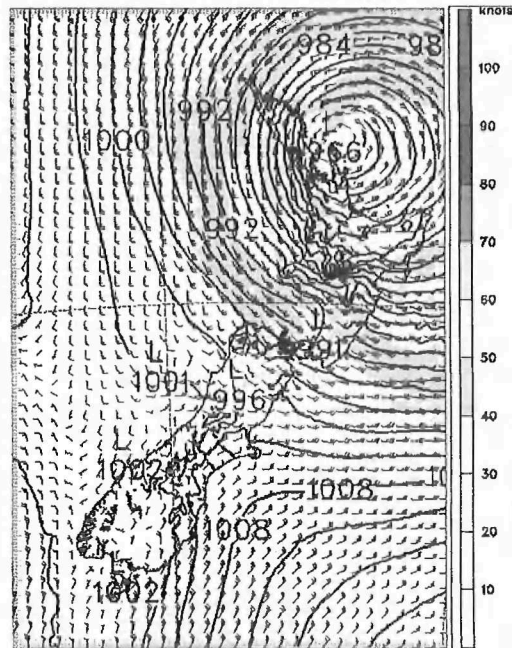

Figure 3: Observed wind gusts (measured in knots, 1 knot = 1.85 km/hr) early in the morning of February 14 2023. Source: MetService.

Aside from extreme hourly rainfall rates (>20mm/hour) persisting for more than six consecutive hours, the human impacts associated with Cyclone Gabrielle were particularly acute over Te Matau-a-Māui and Te Tairāwhiti for multiple reasons. First, the most intense rainfall arrived in the middle of the night, complicating the delivery of emergency messaging and up-to-date information about weather warnings to the public. Second, seven of the ten sites monitoring rainfall and river flows in the heavily-affected Esk Valley region went offline at 1am on Tuesday February 14 after a repeater station relaying the data failed. This severely impacted the ability to monitor fast-changing conditions just as rainfall rates proceeded to nearly double over the following hours (pink line in figure 2b).

Most significantly, access to both electricity and telecommunications was lost for a significant proportion of the population across Te Matau-a-Māui and Te Tairāwhiti at around 8am on February 14 - this coincided with a critical substation (Redclyffe) being inundated with floodwaters (a 2020 report by national grid operator, Transpower, found that Redclyffe was one of twelve locations in their network assessed as highly vulnerable to flooding). At its peak, an estimated 224,000 people - nearly 5% of ANZ's entire population - were lacking electricity across the country, while it was nearly a week before electricity services were restored to most homes.

In addition to the impacts on electricity and telecommunications access, almost all the main roads connecting Te Matau-a-Māui and Te Tairāwhiti with other parts of the country experienced washouts or landslide-related damage, including many bridges along arterial routes. Many critical roads were also closed in other regions in the aftermath of Gabrielle (Table 1), including State Highway 23 linking Raglan with Kirikiriroa (Hamilton), a key section of State Highway 1 linking Tāmaki Makaurau with Te Tai Tokerau, as well as further washouts for State Highway 25a - a key route for communities in Te Tara-O-Te-Ika-A-Māui already closed following the Tāmaki MakaurauAnniversary floods earlier in January. Timescales for when these roads will be fixed vary, though other extreme rainfall events

5

around the country offer insights: significant damage to State Highway 6 between Nelson and Picton was repaired within four months of severe rainfall in August 2022, while a key section of State Highway 60 (over Takaka Hill Road) took nearly four years to be fixed after sustaining damage during Cyclone Gita in 2018.

State Highway Closed in aftermath of Cyclone Gabrielle	Estimated summertime traffic flows (vehicles per day)	Location of traffic flow estimates
1	13000	North of Tāmaki Makaurau (Wellsford)
2	3000	Between Ahuririand Wairoa (Tangoio)
5	4000	Between Taupō and Ahuriri (Te Pohue)
23	5000	Between Raglan & Kirikiriroa
25A*	6000	Between Kopu and Hikuai
35	2500	North of Tologa Bay

Table 1: Traffic flows associated with selected roads which were significantly impacted by Cyclone Gabrielle. *For SH25A, an existing washout from the Tāmaki Makaurau Anniversary floods was exacerbated during Cyclone Gabrielle.

The cyclone's impacts also manifested in damaged houses and evacuations, leaving approximately 10,500 people in displacement situations (IDMC, 2023). 1,335 people were evacuated from Opotiki district due to the heavy storm on 13 Feb as reported by the NZ Herald (2023), equal to nearly 15 percent of the total district population (Opotiki District Council, n.d.). There are also adverse effects from consecutive floods on public health. Experiencing recurring floods is known to affect a population's psychological health and health-related quality of life, leading to higher levels of anxiety, depression, and post traumatic stress syndrome compared to unaffected populations (French et al., 2020). Many long-term impacts are moreover expected for primary industries in the region, with orchards, vineyards, horticulture and crops devastated, some of which were entirely "wiped out" (RNZ, 2023).

According to the Finance Minister, initial estimates of the economic damage linked to Cyclone Gabrielle is on par with the 2011 Ōtautahiearthquake, the country's costliest disaster on record, at roughly NZ$13 billion (Stuff, 2023; BBC, 2023). Acknowledging that annual weather-related insurance claims reached an all-time high of NZ$335 million in 2022 (Stuff, 2023), the multi-billion dollar damage estimation for Cyclone Gabrielle is a significant jump in scale for non-earthquake events.

1.2. External climate drivers and antecedent conditions

La Niña

The El Niño Southern Oscillation is responsible for a significant fraction of interannual summertime rainfall variability over ANZ (figure 4). Typically, the northern and eastern regions of Te Ika-a-Māui - regions which can often have very dry summers - experience higher-than-average rainfall over December to February during a La Niña event, with rainfall anomalies more than 30% above average in some parts of Te Tai Tokerau (based on a composite of past La Niña years).

Summer rainfall during La Niña & El Niño

NIWA

La Niña

El Niño

Summer La Niña years:
1973-74, 1975-76, 1988-89, 1998-99, 1999-00, 2000-01, 2007-08, 2008-09, 2010-11, 2011-12, 2020-21, 2021-22

Summer El Niño years:
1972-73, 1977-78, 1982-83, 1986-87, 1991-92, 1992-93, 1994-95, 1997-98, 2004-05, 2009-10, 2015-16

Rainfall difference from normal (%)

−30   −20   −10   0   10   20   30

Data: NIWA Virtual Climate Station Network (VCSN). Anomalies are calculated with reference to a 1991-2020 climatology. Summer refers to the meteorological season which runs from December-February.
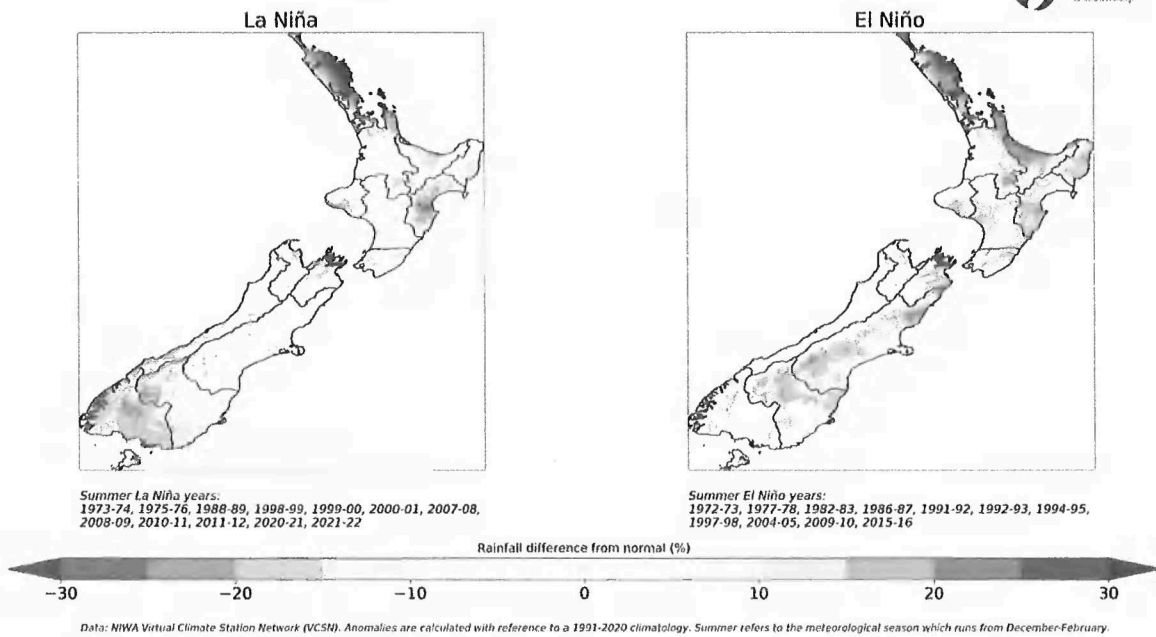
Figure 4: Composite of ENSO rainfall anomalies for the austral summertime (December-February) using high-quality local rainfall data (VCSN). Source: NIWA.

Examples of significant rainfall from other La Niña summers include back-to-back floods in Te Tairāwhiti region on March 23-24 and April 12-13 2022 (which likely compounded the impacts of Cyclone Gabrielle), as well as a sequence of heavy rainfall events in the summer of 2011 - most notably, a two-day extreme rainfall event on January 22-23 2011 caused by Tropical Depression 07F and which also resulted in widespread flooding across Te Ika-a-Māui (figure 5).

Ex-TC Fergus, 30-31 Dec 1996
Whangārei = 168.2 mm
Whitianga = 320.6 mm
Napier = 66.4 mm

Tropical Depression 07F, 22-23 Jan 2011
Whangārei = 115 mm
Whitianga = 148.8 mm
Napier = 139.4 mm

Ex-TC Gabrielle, 13-14 Feb 2023
Whangārei = 287.3 mm
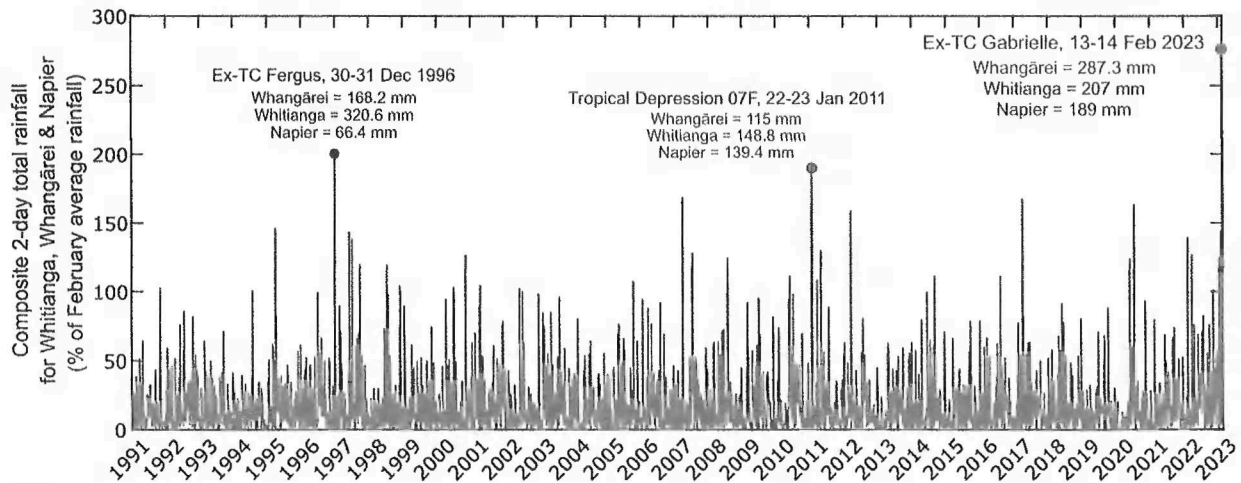Whitianga = 207 mm
Napier = 189 mm

Figure 5: Normalised two-day rainfall anomalies across three stations (Whangārei, Te Tai Tokerau; Whitianga, Te Tara-O-Te-Ika-A-Māui; Ahuriri (Napier) Airport, Te Matau-a-Māui) from 1991 to 2023. Data normalised with respect to February-mean rainfall at each station before combining to form a composite percentage anomaly.

However, it is worth noting that other ex-TC events have also exhibited impacts with a regional footprint similar to Cyclone Gabrielle without coinciding with La Niña conditions: most notably, the summer associated with Cyclone Bola, 1987/88, coincided with strong El Niño conditions. Similarly, Cyclone Fergus caused significant wind- and rain-related impacts across the Te Tai Tokerau, Waikato and Te Moana-a-Toi regions in late December 1996 (see figure 5) despite that summer exhibiting ENSO-neutral conditions.

Marine heatwaves

Across the wider ANZ region, strong marine heatwave conditions persisted throughout the summer of 2022/23. While the strongest epicentres of the ongoing marine heatwave were concentrated further to the south than the regions most affected by the impacts of Cyclone Gabrielle, sea surface temperatures were still several degrees warmer than average across the moisture source regions of Gabrielle. All things equal, this would have likely helped the system to maintain its strength as well as offering a richer source of moisture to precipitate out as extreme rainfall (Trenberth *et al.* 2018).

Compounding role of previous events

Only two weeks prior to the arrival of Cyclone Gabrielle, Aotearoa experienced its costliest ever extreme rainfall event in the form of the Tāmaki MakaurauAnniversary floods: this pluvial flooding event brought widespread devastation to Te Tai Tokerau but particularly across Tāmaki Makaurau, the largest city in the country. Earlier in January, Cyclone Hale also resulted in significant rainfall across many regions of Te Ika-a-Māui. In fact, it was the wettest January on record for nearly all locations in Te Ika-a-Māui which were subsequently impacted by Gabrielle (see figure 6): such antecedent conditions can be expected to have exacerbated the speed with which rivers rose and the number of landslides which occurred in the aftermath of Gabrielle.
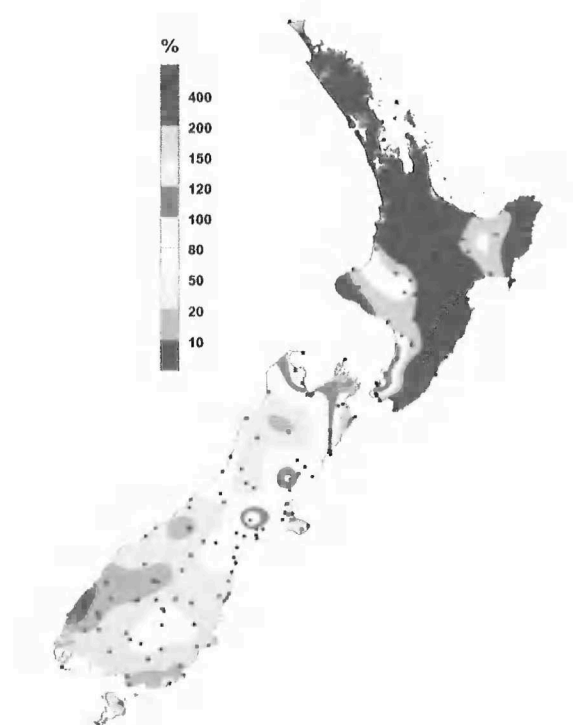
Figure 6: Observed monthly rainfall anomalies for the month of January 2023 (expressed with respect to a 1991-2020 climatology). Source: NIWA.

1.3. Previous studies on extreme rainfall and tropical cyclone responses to climate change over the ANZ region

Generally, there is an expectation of slightly fewer tropical cyclones with climate change in the southern hemisphere, but with an increase in the proportion of events reaching category 3 or above as well as increases in the speed with which tropical cyclones intensify (Roberts *et al.* 2020). Emerging

observational evidence points to the frequency of tropical cyclones slightly decreasing over the South Pacific basin (Chand *et al.* 2022). Knutson *et al.* (2020) similarly estimated a 20% reduction in TC frequency over the South-west Pacific basin after 2°C of warming relative to a pre-industrial climate, albeit with high levels of uncertainty. However, Chapter 11 of the IPCC's AR6 Working Group 1 also concludes "it is likely that the global proportion of Category 3–5 tropical cyclone instances has increased over the past four decades", though evidence of such trends is not yet robust for regions outside the North Atlantic. Similarly, recent work by Bhatia *et al.* (2022) has found, globally, that the thermodynamic environments around tropical cyclones have become more favourable for rapid intensification and human-induced warming has increased the probability of such rapid intensification occurring. However, specific results were not available for the South Pacific region due to inconsistencies in historical trends between different observational datasets.

Other studies have attempted to perform more targeted attribution studies for past tropical cyclone events. One of the most comprehensive studies by Patricola and Wehner (2018) found negligible changes in peak wind speeds associated with Hurricanes Katrina, Irma or Maria, when comparing high-resolution, highly-conditioned simulations of these events in the climate of 1996-2016 relative to if they occurred in a pre-industrial climate (peak winds did increase by 10-15% when repeating the experiments under a very high warming (end-of-century, RCP8.5) scenario). Similarly, robust reductions of the TC's minimum sea level pressure (SLP) were found when comparing future warming scenarios with the current climate: for example, the authors found TC Yasi (which impacted Queensland in 2011) would have had a minimum SLP ~10hPa lower under conditions consistent with the end-of-century climate under an RCP4.5 scenario relative to the current climate. However, no statistically significant reductions in central pressure minima were identified for simulations of events in the current climate with corresponding simulations in a pre-industrial climate.

So while it is likely that the minimum SLP and peak wind speeds associated with tropical cyclones will both intensify if global temperatures continue to increase unabated, there is not sufficient evidence that such changes are detectable based on the warming observed to date.

However, the opposite is true when considering rainfall associated with these weather systems, with the Sixth Assessment Report of the Intergovernmental Panel on Climate Change (IPCC) concluding, with high confidence, that rainfall associated with tropical cyclones, extra-tropical cyclones and atmospheric rivers (and in severe convective storms in some regions) will increase with climate change.

Event attribution studies of TCs provide evidence of increased rainfall associated with anthropogenic influence (IPCC AR6). Peak TC rainfall rates increase by at least the Clausius-Clapeyron rate of 7%/degree of local warming; however, in some cases this rate can be exceeded because of increased low-level moisture convergence associated with increasing TC wind intensity. Event attribution studies of rainfall in the Aotearoa region do not provide accounts of TCs *per se* – however, a few studies do provide information on extreme rainfalls such as resulted from decaying TCs, severe low pressure systems and atmospheric river events, which might reasonably be considered to provide additional lines of similar information. Dean et al. (2013) found an attributable increase in the moisture associated with two days of extreme rainfall which caused significant flooding in Golden Bay in December 2011. Rosier et al. (2015) likewise concluded that human influence made the 5-day rainfalls that flooded Te Tai Tokerau in 2014 both more intense and more likely. Stone et al. (2022) reported attribution results for four extreme rainfall events, all of which revealed attributable increases in rainfall amounts, albeit with differing confidence resulting from differing numbers of simulations that reliably reproduced the processes involved: (i) ex-TC Debbie (April 2017, Te Ika-a-Māui) revealed a 0-15% rainfall magnitude

shift, (ii) extreme rain in Otago (July 2017) showed similar results but with fewer simulations deemed reliable, (iii) extreme rain in Canterbury (May 2021) showed a magnitude shift of 5-10% but again with fewer reliable models, and (iv) Buller, on the West Coast (July 2021) extreme rainfall was reported as 10% more intense due to human influence, and with greater confidence as more models could be utilised.

Further rainfall events were examined by Frame et al. (2020) (see also Frame et al. (2018)), who estimated, for the first time, the attributable portion of the costs of damaging extreme weather events. They examined twelve extreme rainfall events that led to flooding in Aotearoa over the decade 2007-2017 (one of which was in common with Stone et al. above). Focusing on an assessment of changes in the likelihood of each event occurring, not any changes in event magnitude, most events exhibited a best-guess probability ratio of about 1.4, meaning the event was 40% more likely due to anthropogenic climate change. However, there was some regional variation, with two events (in Otago and the Lower Te Ika-a-Māui, respectively occurring in early- and late-June 2015) showing no significant change in likelihood.

The aggregate picture of extreme rainfall attribution in the Aotearoa region gained from studies to date appears to be that, when such events occur, the rainfall they bring is more intense than it otherwise would have been in the absence of human influence. How that translates to corresponding changes in the frequency in such events is more sensitive to model uncertainty as well as the framing of each attribution analysis.

1.4. Selecting an event definition

While the impacts associated with Cyclone Gabrielle were widespread and significant for many regions, the epicentre of the devastation - including major impacts to multiple sets of "lifeline" infrastructure - were primarily concentrated across Te Matau-a-Māui and Te Tairāwhiti regions, where the majority of the rain fell within 48 hours. We have therefore chosen to restrict our analysis to two-day extreme rainfall averaged over both these regions.

The decision to analyse both Te Tairāwhiti and Te Matau-a-Māui together, rather than separately, depends in part on constraints provided by currently available model resolution, and the current ability (or inability) of models to offer a coherent assessment of attributable rainfall differences at finer scales. Smaller-scale study regions should be analysed as more detailed, more reliable modelling becomes available. Cyclone Gabrielle was, however, large enough to deliver significant impacts to both Te Tairawhiti and Te Matau-a-Māui regions together, justifying our choice to analyse both regions together in this rapid study.

There are of course other regions affected by flooding, and thus future studies might want to focus on impacts across multiple distinct regions from the same weather system - but this is beyond scope for a rapid attribution analysis, in particular as some of the impacts in the Tararua district were complicated by the fact that the main river catchment (Manawatū) flows to the other side of the mountain ranges relative to where the rain fell. Our event definition does also exclude impacts in Te Tai Tokerau that were wind-related, and likely heavily exacerbated from saturated land and unstable hill slopes associated with the Tāmaki MakaurauAnniversary floods (whereas most of the impacts in Te Matau-a-Māui and Te Tairāwhiti were more likely related to the rain which fell from Gabrielle itself).

1 0

Figure 7 shows the 2-day accumulated rainfall during 13-14 Feb, 2023 over Aotearoa seen in MSWEP, a global precipitation product with a 3-hourly 0.1° resolution available from 1979 to ~3 hours from real-time (see Section 2.1.2). The heaviest rainfall during this period fell in Te Matau-a-Māui and Te Tairāwhiti, on the east coast of Te Ika-a-Māui, bounded by the Kaimanawa and Raukūmara mountain ranges on the west, and the south Pacific Ocean on the east. Incidentally, these regions are among the areas that were severely hit by floods during Cyclone Gabrielle. Therefore, by selecting a study domain over these regions (red highlight in Fig. XX; hereafter referred to as Te Matau-a-Māui/Te Tairāwhiti), we define the event as the annual maximum of the 2-day accumulated rainfall, area-averaged over the study region, defining the year as July-June so as to centre on the South Pacific cyclone season (November-April).
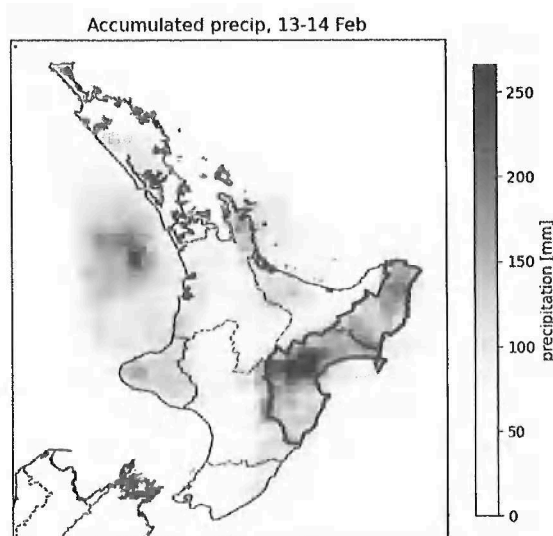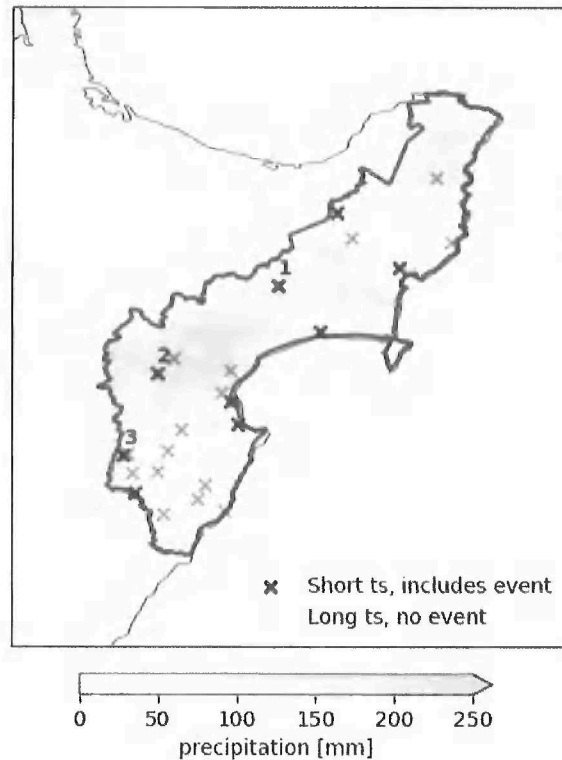

Figure 7: 2-day accumulated precipitation [mm] from Cyclone Gabrielle in the MSWEP data. The red highlight shows the study region - Te Matau-a-Māui/Te Tairāwhiti, on the east coast of Aotearoa's Te Ika-a-Māui.

2 Data and methods

2.1 Observational data

2.1.1 Station data

24 stations operated by either the National Institute of Water and Atmospheric Research Ltd (NIWA) or the Metservice and sourced from the NIWA National Climate Database are identified in the study region (locations shown by 'x' in Fig. 8). Many of the automated weather stations at these sites lost power during the cyclone and as a result, only 6 of these stations currently record observations of the event; the earliest records at these stations begin in 1990. 15 of the 18 remaining stations have observations as far back as the year 1979. Therefore, we use the station records primarily for evaluating the gridded dataset which we identified for defining the event (details in Section 2.2). In addition to these records, we include rainfall records from three stations operated by the council which recorded the event (numbered 1-3 alongside 'x' in Fig. 8).

Fig. 8: 2-day accumulated precipitation [mm] from Cyclone Gabrielle in the MSWEP data with station locations overplotted. The red highlight shows the study region- Te Matau-a-Māui/Te Tairāwhiti, on the east coast of Aotearoa's Te Ika-a-Māui.

2.1.2 Gridded datasets

We use the Multi-Source Weighted-Ensemble Precipitation (MSWEP) v2.8 dataset as the primary dataset for calculating the trend and return period of the 2022 event for the attribution analysis. The MSWEP dataset (updated from Beck et al., 2019) is fully global, available at 3-hourly intervals, and at 0.1° spatial resolution, available from 1979 to ~3 hours from real-time. This product combines gauge-, satellite-, and reanalysis-based data for reliable precipitation estimates, globally. The data used in this analysis were downloaded on February 20th, at which time it is known that observations of the event were unavailable at some station locations, and so there is some uncertainty about the representation of the event itself in this dataset.

2.1.3 Composite observations

For additional comparison with the regionally averaged MSWEP total rainfall we have also constructed a regional average rainfall product based solely on 11 composite rainfall stations with records that go back to at least 1969 (locations in Fig 9). This is constructed from a total of 30 stations, either based on station replacement at the same location, such as changes from manual to automatic records, or sufficiently co-located overlapping records. All of these stations include the event and were selected to be geographically as representative as possible. As with MSWEP, the reliability of this method for capturing a regional rainfall total is uncertain, due to both the merging and the significant under sampling of high elevations.
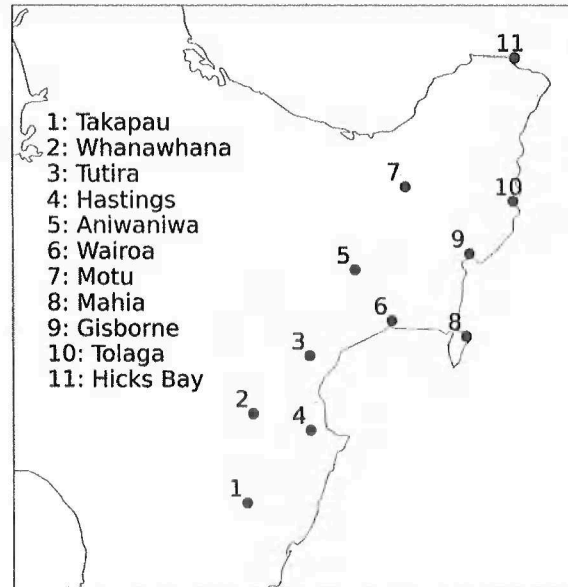
Fig. 9:Locations and names of 11 composite station records used to estimate a daily regional mean rainfall.

2.1.4 Observed global mean surface temperature

Lastly, as a measure of anthropogenic climate change we use the (low-pass filtered) global mean surface temperature (GMST), where GMST is taken from the National Aeronautics and Space Administration (NASA) Goddard Institute for Space Science (GISS) surface temperature analysis (GISTEMP, Hansen et al., 2010 and Lenssen et al. 2019).

2.2 Model and experiment descriptions

Across all climate modelling frameworks used, there was a requirement that model resolution was sufficiently high for the complexities of ANZ's topography to be reasonably well-represented - this requirement explains why CMIP6 models were excluded from all subsequent analysis.

We use four multi-model ensembles from climate modelling experiments using very different framings (Philip et al., 2020): Sea Surface temperature (SST) driven global circulation high resolution models, coupled global circulation models and regional climate models.
Specifically:

1. **CORDEX:** Coordinated Regional Climate Downscaling Experiment for Australasia (CORDEX-AUS) - we use 9 models at 0.22° resolution (AUS-22) multi-model ensemble (Di Virgilio et al., 2019; Evans et al., 2020) , comprising of simulations resulting from pairings of Global Climate Models (GCMs) and Regional Climate Models (RCMs). These simulations are composed of historical simulations up to 2005, and extended to the year 2100 using the RCP8.5 scenario. Models at 0.44° resolution (AUS-44) were found to be unable to represent the orographic rainfall over the region and so were excluded from the study.

2. **GFDL high-resolution models:** The FLOR (Vecchi et al. 2014) and AM2.5C360 (Yang et al. 2021, Chan et al. 2021) climate models are developed at Geophysical Fluid Dynamics Laboratory (GFDL). The FLOR model is an atmosphere-ocean coupled GCM with a resolution of 50 km for land and atmosphere and 1 degree for ocean and ice. Ten ensemble simulations

/3

from FLOR are analysed, which cover the period from 1860 to 2100 and include both the historical and RCP4.5 experiments driven by transient radiative forcings from CMIP5 (Taylor et al. 2012). The AM2.5C360 is an atmospheric GCM based on that in the FLOR model (Delworth et al. 2012, Vecchi et al. 2014) with a horizontal resolution of 25 km. Three ensemble simulations of the Atmospheric Model Intercomparison Project (AMIP) experiment (1871-2050) are analysed. These simulations are initialised from three different pre-industrial conditions but forced by the same SSTs from HadISST1 (Rayner et al. 2003) after groupwise adjustments (Chan et al. 2021) over 1871-2020. SSTs between 2021 and 2050 are using the FLOR RCP4.5 experiment 10-ensemble mean values after bias correction. Radiative forcings are using historical values over 1871-2014 and RCP4.5 values after that.

3. **HighResMIP:** SST-forced model ensemble (Haarsma et al. 2016), the simulations for which span from 1950 to 2050. The SST and sea ice forcings for the period 1950-2014 are obtained from the 0.25° x 0.25° Hadley Centre Global Sea Ice and Sea Surface Temperature dataset that have undergone area-weighted regridding to match the climate model resolution (see Table B). For the 'future' time period (2015-2050), SST/sea-ice data are derived from RCP8.5 (CMIP5) data, and combined with greenhouse gas forcings from SSP5-8.5 (CMIP6) simulations (see Section 3.3 of Haarsma et al. 2016 for further details).

4. **CCAM:** CSIRO Conformal-Cubic Atmospheric Model (CCAM) (Thatcher and McGregor, 2009; McGregor and Dix, 2008). This ensemble consists of 10 initial condition ensemble members, driven by OSTIA SST and sea ice and at 12km resolution over Aotearoa, for the period 1982-2020. The year 1981 is used for spin up and not subsequently analysed. Historical forcings from CMIP6 are used for the period 1982-2014 followed by SSP245 forcings for the period 2015-2020. The model is run globally with a stretched grid configuration enabling relatively high resolution over the entire South Pacific domain (12-35km).

2.3 Statistical methods

In this analysis we analyse time series of precipitation averaged over Te Matau-a-Māui/Te Tairāwhiti of RX2day values. Methods for observational and model analysis and for model evaluation and synthesis are used according to the World Weather Attribution Protocol, described in Philip et al. (2020), with supporting details found in van Oldenborgh et al. (2021), Ciavarella et al. (2021) and here.

The analysis steps include: (i) trend calculation from observations; (ii) model evaluation; (iii) multi-method multi-model attribution and (iv) synthesis of the attribution statement.
We calculate the return periods, Probability Ratio (PR; the factor-change in the event's probability) and change in intensity of the event under study in order to compare the climate of now and the climate of the past, defined respectively by the GMST values of now and of the preindustrial past (1850-1900, based on the Global Warming Index). For the past climate we use a difference in GMST of -1.2°C, and to compare the current climate with a future, warmer world we use a difference in GMST of 0.8°C. To statistically model the event under study, we use a GEV that scales with GMST. Next, results from observations and models that pass the validation tests are synthesized into a single attribution statement.

3 Observational analysis: return period and trend

3.1 Analysis of point station data

3.1.1 Evaluation of gridded dataset

Fig. 10 shows the time series of annual maximum 2-day accumulated rainfall for each of the 24 stations shown by the black plots in Fig. 8. The pink dot corresponds to the Feb 13-14, 2023 estimate, wherever available. The corresponding values from the nearest MSWEP grid cell are shown in blue. Stations are ordered from north-south, with stations including the event (black crosses in the map above) grouped together first. Although MSWEP does not capture the most extreme rainfall at high elevations (see stations numbered 1, 2 and 3 in Fig. 10) there is a general agreement between the gridded product and the station-based rainfall data for all but the most extreme events, thus justifying the choice of MSWEP for event definition.
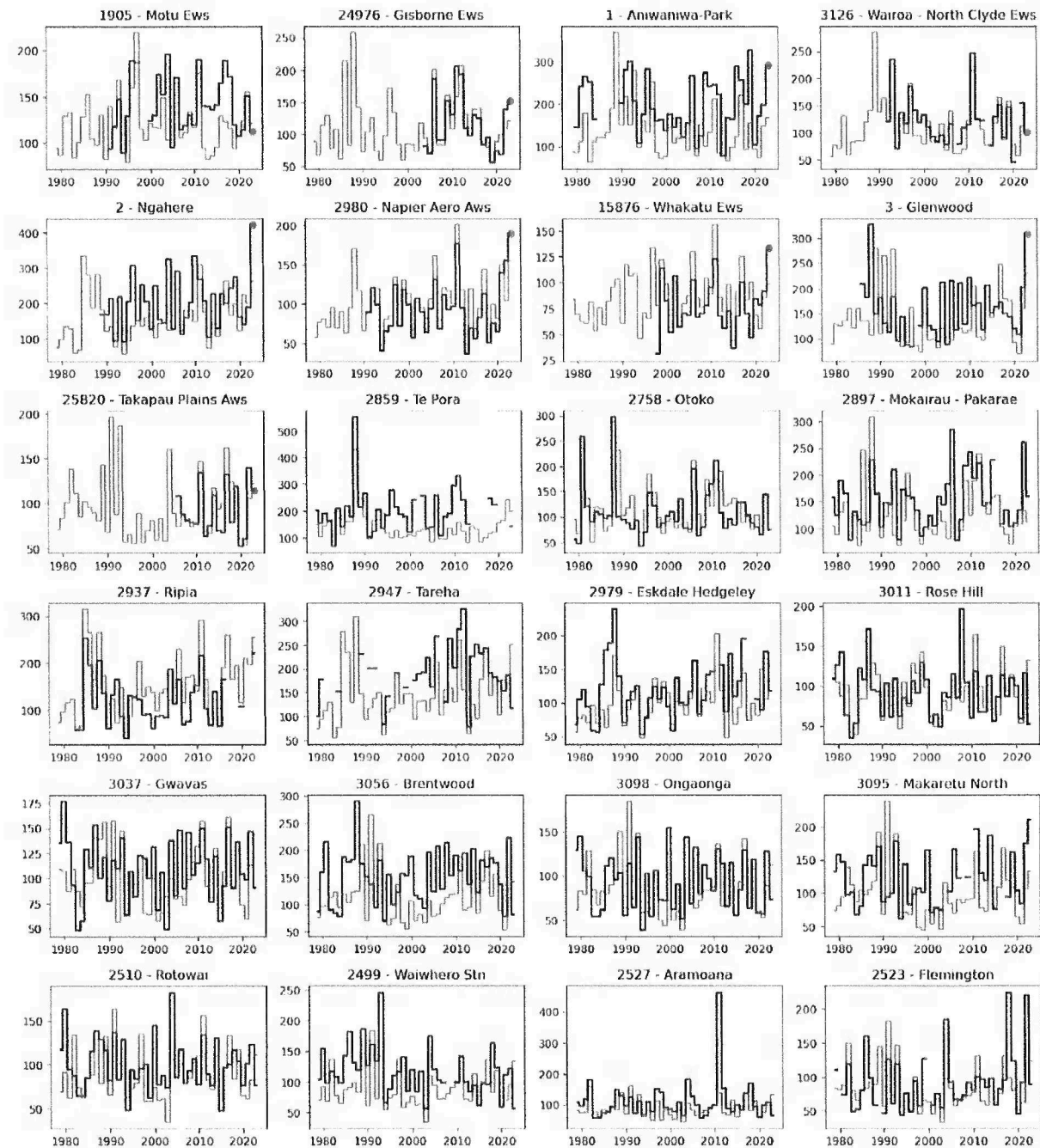

Fig. 10: time series over 24 different stations. Black: station data; Blue: MSWEP data at the nearest grid point. Pink circles are the value for the event.

15

3.2 Analysis of gridded data

Fig. 11(a) shows the response of the observed annual maximum of 2-day accumulated rainfall (based on MSWEP) area-averaged over the study region to global mean temperature. There is a seemingly increasing tendency of higher rainfall extremes in this region due to global warming. However, owing to the short length of the observed data (~43 years), it is necessary to repeat the analysis with climate models that can reliably simulate the climate of the region for a clear attribution of this signal to climate change.

Fig. 11(b) shows the return period curves in the present, 2023 climate and the past climate when the global mean temperature was 1.2 °C cooler. The best-estimated return period of the 2023 event averaged over the study region is 11 years (5-45 years), as shown in Fig. 5(b), which we round to an average 1-in-10 years for the attribution analysis. The event is 4 times more likely in the 2023 climate. However, this estimate is not statistically significant with an uncertainty range of [0.4, 3300]. Further, the rainfall is found to be 31% more intense in the current climate, but once again, this estimate is not statistically significant (uncertainty range: -17% to 130%).
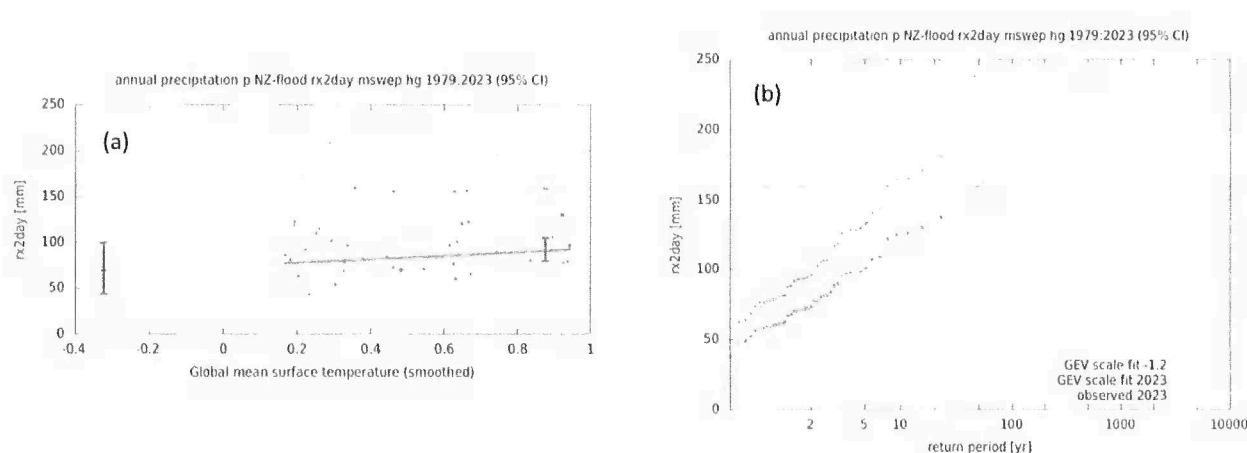

Fig. 11: GEV fit with constant dispersion parameters, and location parameter scaling proportional to GMST of the index series, for Te Matau-a-Māui/Te Tairāwhiti region based on MSWEP dataset. The 2023 event is included in the fit. (a) Observed annual (July-Jun) annual 2-day average rainfall as a function of the smoothed GMST. The thick red line denotes the time-varying location parameter. The vertical red lines show the 95% confidence interval for the location parameter, for the current, 2022 climate and a 1.2°C cooler climate. The 2023 observation is highlighted with the magenta box. (b) Return time plots for the climate of 2023 (red) and a climate with GMST 1.2 °C cooler (blue). The past observations are shown twice: once shifted up to the current climate and once shifted down to the climate of the late nineteenth century. The markers show the data and the lines show the fits and uncertainty from the bootstrap. The magenta line shows the magnitude of the 2023 event analysed here.

3.3 Sensitivity of return period to choice of observational product

When the same analysis is applied to the averaged composite station record the best-estimated return period of the 2023 event averaged over the study region is 89 years (MSWEP=11) with a change in intensity of -21% (MSWEP=32%) and a probability ratio of 0.4 (MSWEP=4.4). Fits to the two records are compared in Figure 12. In the composite record the events of 13-14th February are the largest 48-hour rainfall event since Cyclone Bola in 1988. The decreasing trend seen in the composite record is caused by the selection of observation stations that sample the extremely high rainfall observed over the high and complex orography of the region (see figure S9), but which do not form a representative sample of local trends; whereas MSWEP captures longer-term trends over the region as a whole. This

implies a possible underestimate of the event itself by MSWEP, either due to an absence of station data in the near-real time estimates or problems in the way MSWEP merges multiple rainfall products with exceptionally extreme events. It is also worth considering that while our best estimates of the return period for the entire region are between 11 and 89 years, return periods within individual catchments are likely much higher (Appendix 1).
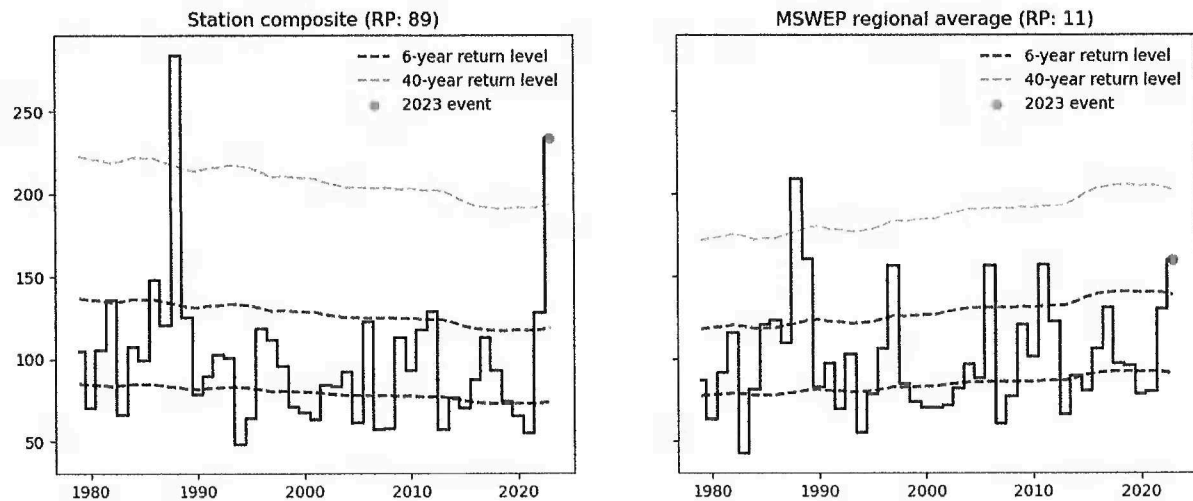
Fig. 12: Observed annual (July-Jun) annual maximum 2-day rainfall for the composite station record (left) and MSWEP (right). Overplotted are the best time variant trend (black dashes) as well as return period estimates for the 1 in 6-year and 1 in 40-year return level.

4 Model evaluation

Table 2 below shows the results of the model validation for Te Matau-a-Māui/Te Tairāwhiti region. The climate models are evaluated against the observations in their ability to capture:

1. Spatial patterns: Models that do not match the observations in terms of the large-scale precipitation patterns are excluded. In this case in particular we exclude models that do not show a distinctly higher precipitation towards the east of the mountains.

2. Parameters of the fitted GEV models. We discard the model if the model and observation parameters ranges do not overlap.

The models were not evaluated in terms of how well they capture the seasonal cycle over the region because historical records show that extreme rainfall has the potential to occur throughout most of the year. The models are labelled as 'good','reasonable', or 'bad' based on their performances in terms of the three criteria discussed above.

17

Table 2. Model evaluation values for the statistical parameters and spatial pattern.

Observations	Spatial pattern	Dispersion	Shape	Event magnitude [mm]
MSWEP (1979-2022)		0.289 (0.205 ... 0.346)	0.073 (-0.21 ... 0.42)	159.84
Model				**Threshold for 10-yr return period**
AM2.5C360	good	0.268 (0.233 ... 0.294)	-0.068 (-0.19 ... 0.084)	114.23
FLOR	reasonable	0.261 (0.244 ... 0.278)	-0.057 (-0.12 ... -0.0010)	86.972
HadGEM2-ES_r1_CCLM5-0-15	reasonable	0.242 (0.179 ... 0.291)	-0.20 (-0.51 ... -0.039)	201.77
HadGEM2-ES_r1_RegCM4-7	good	0.204 (0.152 ... 0.227)	-0.22 (-0.47 ... 0.10)	61.182
HadGEM2-ES_r1_REMO2015	good	0.231 (0.175 ... 0.270)	-0.038 (-0.20 ... 0.14)	207.28
MPI-ESM-LR_r1_CCLM5-0-15	good	0.267 (0.189 ... 0.313)	-0.13 (-0.45 ... 0.028)	242.96
MPI-ESM-LR_r1_REMO2015	good	0.231 (0.183 ... 0.259)	-0.21 (-0.55 ... 0.032)	207.79
MPI-ESM-MR_r1_RegCM4-7	good	0.234 (0.145 ... 0.278)	0.067 (-0.14 ... 0.39)	194.5
NorESM1-M_r1_CCLM5-0-15	reasonable	0.247 (0.183 ... 0.287)	-0.027 (-0.31 ... 0.18)	190.53
NorESM1-M_r1_RegCM4-7	good	0.245 (0.183 ... 0.301)	0.025 (-0.25 ... 0.19)	141.73
NorESM1-M_r1_REMO2015	good	0.228 (0.170 ... 0.266)	-0.13 (-0.36 ... 0.080)	177.77
CSIRO-CCAM	good	0.306 (0.289 ... 0.335)	-0.030 (-0.097 ... 0.059)	123.61
CMCC-CM2-VHR4	good	0.282 (0.219 ... 0.321)	-0.031 (-0.32 ... 0.13)	113.008
CNRM-CM6-1-HR	good	0.227 (0.170 ... 0.259)	-0.14 (-0.44 ... 0.033)	123.834
EC-Earth3P-HR	good	0.255 (0.199 ... 0.299)	0.096 (-0.18 ... 0.26)	94.494
HadGEM3-GC31-HM	good	0.288 (0.216 ... 0.337)	0.049 (-0.17 ... 0.20)	133.078
HadGEM3-GC31-MM	bad	0.338 (0.253 ... 0.388)	-0.12 (-0.35 ... 0.13)	116.528
MPI-ESM1-2-XR	good	0.314 (0.237 ... 0.368)	0.043 (-0.14 ... 0.21)	90.472

5 Multi-method multi-model attribution

Table 3 shows Probability Ratios and change in event intensity ΔI in the climate models that have been identified as 'reasonable' or 'good'.

18

Table 3: Probability ratio and change in intensity in RX2D precipitation over Te Matau-a-Māui/Te Tairāwhiti region for models that passed the validation tests,

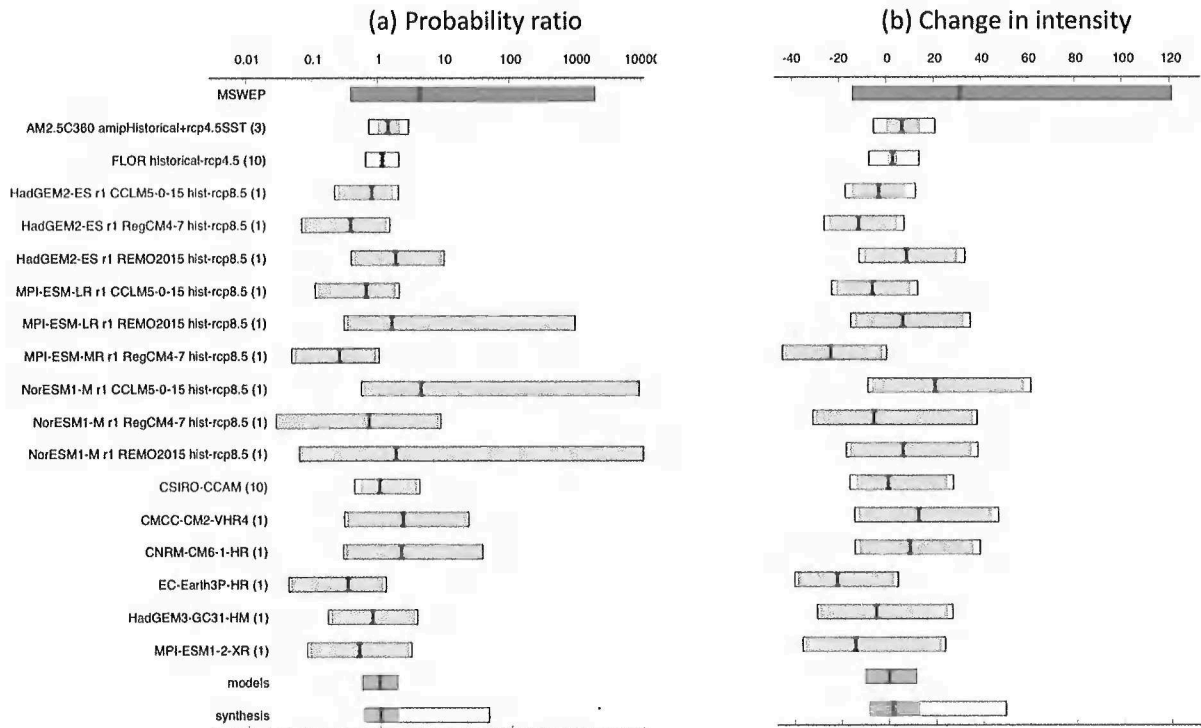| Model / Observations	a. Past vs. present		b. Present vs. future	
	Probability ratio PR [-]	Change in intensity ΔI [%]	Probability ratio PR [-]	Change in intensity ΔI [%]
MSWEP	4.4 (0.39 ... 2.0e+3)	31 (-14 ... 1.2e+2)		
AM2.5C360 amipHistorical+rcp4.5SST (3)	1.5 (1.0 ... 2.2)	6.7 (0.23 ... 14)	1.3 (1.0 ... 1.6)	4.2 (0.14 ... 8.3)
FLOR historical-rcp4.5 (10)	1.2 (1.1 ... 1.3)	2.8 (1.0 ... 4.5)	1.1 (1.0 ... 1.2)	1.8 (0.62 ... 3.0)
HadGEM2-ES_r1_CCLM5-0-15 hist-rcp8.5 (1)	0.81 (0.25 ... 1.7)	-3.1 (-14 ... 7.8)	0.93 (0.61 ... 1.3)	-0.87 (-4.7 ... 3.0)
HadGEM2-ES_r1_RegCM4-7 hist-rcp8.5 (1)	0.38 (0.075 ... 1.3)	-12 (-24 ... 4.4)	0.92 (0.60 ... 1.2)	-1.3 (-5.9 ... 3.0)
HadGEM2-ES_r1_REMO2015 hist-rcp8.5 (1)	1.9 (0.44 ... 9.1)	8.4 (-9.3 ... 29)	1.3 (0.96 ... 1.8)	4.7 (-0.56 ... 9.2)
MPI-ESM-LR_r1_CCLM5-0-15 hist-rcp8.5 (1)	0.65 (0.12 ... 1.8)	-6.1 (-21 ... 9.7)	1.3 (0.72 ... 2.4)	3.1 (-2.7 ... 8.4)
MPI-ESM-LR_r1_REMO2015 hist-rcp8.5 (1)	1.6 (0.33 ... 9.4e+2)	6.6 (-13 ... 32)	1.8 (1.3 ... 3.2)	9.5 (3.3 ... 15)
MPI-ESM-MR_r1_RegCM4-7 hist-rcp8.5 (1)	0.25 (0.051 ... 0.89)	-24 (-44 ... -2.3)	0.78 (0.38 ... 1.8)	-3.0 (-9.8 ... 3.6)
NorESM1-M_r1_CCLM5-0-15 hist-rcp8.5 (1)	4.4 (0.59 ... 8.8e+3)	20 (-6.4 ... 58)	1.1 (0.85 ... 1.4)	2.5 (-3.2 ... 8.6)
NorESM1-M_r1_RegCM4-7 hist-rcp8.5 (1)	0.70 (0.029 ... 8.0)	-5.7 (-31 ... 36)	1.4 (0.077 ... 28)	-5.7 (-31 ... 41)
NorESM1-M_r1_REMO2015 hist-rcp8.5 (1)	1.8 (0.063 ... 1.0e+6)	6.4 (-16 ... 35)	0.99 (0.58 ... 1.4)	-0.24 (-6.9 ... 5.9)
CSIRO-CCAM (10)	1.0 (0.52 ... 3.7)	0.19 (-13 ... 25)	*<not computed>*	*<not computed>*
CMCC-CM2-VHR4 (1)	2.3 (0.32 ... 21)	13 (-12 ... 44)	*<not computed>*	*<not computed>*
CNRM-CM6-1-HR (1)	2.1 (0.31 ... 35)	9.1 (-12 ... 36)	*<not computed>*	*<not computed>*
EC-Earth3P-HR (1)	0.33 (0.044 ... 1.1)	-22 (-39 ... 2.3)	*<not computed>*	*<not computed>*
HadGEM3-GC31-HM (1)	0.77 (0.18 ... 3.3)	-5.2 (-29 ... 25)	*<not computed>*	*<not computed>*
MPI-ESM1-2-XR (1)	0.48 (0.084 ... 2.7)	-14 (-35 ... 22)	*<not computed>*	*<not computed>*

6 Hazard synthesis

For the event definitions described above we evaluate the influence of anthropogenic climate change on the event by calculating the probability ratio as well as the change in intensity using observations and climate models. Models which do not pass the validation tests described above are excluded from the analysis. The aim is to synthesise results from models that pass the evaluation along with the observations-based products, to give an overarching attribution statement. Fig. 13 shows the changes in
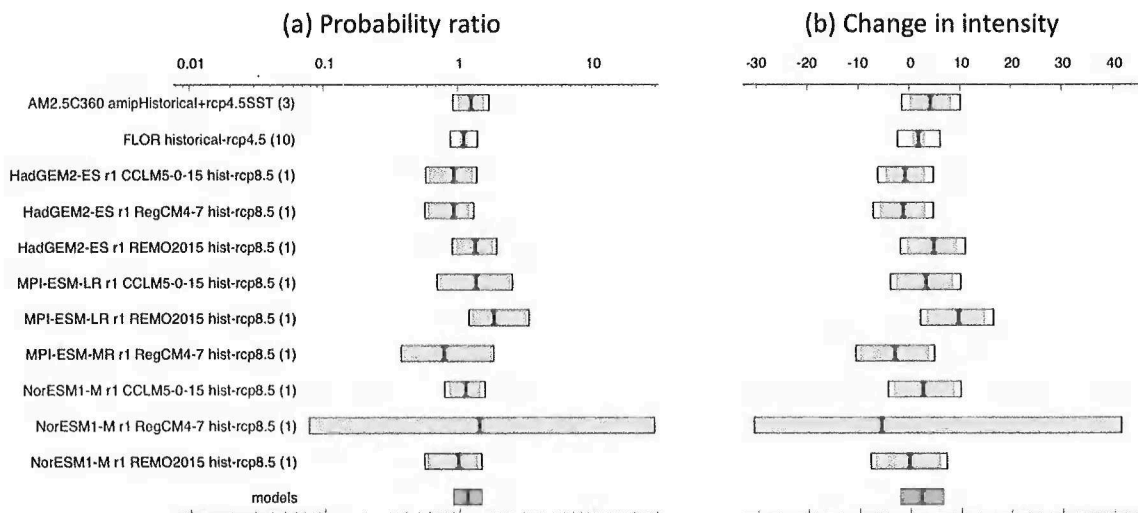
13

probability (left-hand side) and intensity (right-hand side) for the observations (blue) and models (red). To combine them into a synthesised assessment, a term to account for intermodel spread is added (in quadrature) to the natural variability of the models. This is shown in the figures as white boxes around the light red bars. The dark red bar shows the model average, consisting of a weighted mean using the (uncorrelated) uncertainties due to natural variability. The observations and models are combined into a single result in two ways. Firstly, we neglect common model uncertainties beyond the intermodel spread that is depicted by the model average, and compute the weighted average of models (dark red bar) and observations (dark blue bar): this is indicated by the magenta bar. As, due to common model uncertainties, model uncertainty can be larger than the intermodel spread, secondly, we also show the more conservative estimate of an unweighted, direct average of observations (dark red bar) and models (dark blue bar) contributing 50% each, indicated by the white box around the magenta bar in the synthesis figures.

The observations, in this case MSWEP, show a best estimate suggesting a strong increase in intensity and likelihood of the event occurring which is not represented in the model results. The weighted synthesised change in likelihood and probability suggest no significant change. The unweighted changes however do show an upper bound of an increase in probability of a factor of 100 while the upper bound of the intensity change is 40%. Given that not only the MSWEP data but also individual stations show an increase in likelihood and intensity due to climate change and an increase in extreme precipitation on short timescales is what we expect and see globally in a warming world, the models and thus the synthesised result probably underestimate the role of climate change. Natural variability adds noise to any climate change signal and can produce trends where sampling frequency (amount of data) is too low, however it is very unlikely that the positive observational best estimate here results from natural variability alone. There is no further known reason for the trend in observations other than climate change, hence the true change in intensity and likelihood in the event attributable to climate change is presumably better described by the unweighted synthesised bounds, depicted by the white box around the magenta one in figure 13. We therefore cannot quantify the overarching role of climate change but conclude that the direction of change is to increase the intensity and likelihood of RX2day events.

This conclusion is further corroborated by analysing how the likelihood and intensity of the above defined event is changing in a 2C warmer world (0.8C warmer than today). Figure 14 shows the results for those models that have future simulations as well as a combined model results, derived identically to the past-present results. While the changes are still not significant, the best estimate does show an increase in likelihood and probability, suggesting that natural variability and dynamical processes that currently mask the thermodynamic warming in the models become less dominant with further warming.

(a) Probability ratio

0.01 0.1 1 10 100 1000 10000

MSWEP

AM2.5C360 amipHistorical+rcp4.5SST (3)

FLOR historical-rcp4.5 (10)

HadGEM2-ES r1 CCLM5-0-15 hist-rcp8.5 (1)

HadGEM2-ES r1 RegCM4-7 hist-rcp8.5 (1)

HadGEM2-ES r1 REMO2015 hist-rcp8.5 (1)

MPI-ESM-LR r1 CCLM5-0-15 hist-rcp8.5 (1)

MPI-ESM-LR r1 REMO2015 hist-rcp8.5 (1)

MPI-ESM-MR r1 RegCM4-7 hist-rcp8.5 (1)

NorESM1-M r1 CCLM5-0-15 hist-rcp8.5 (1)

NorESM1-M r1 RegCM4-7 hist-rcp8.5 (1)

NorESM1-M r1 REMO2015 hist-rcp8.5 (1)

CSIRO-CCAM (10)

CMCC-CM2-VHR4 (1)

CNRM-CM6-1-HR (1)

EC-Earth3P-HR (1)

HadGEM3-GC31-HM (1)

MPI-ESM1-2-XR (1)

models

synthesis

(b) Change in intensity

-40 -20 0 20 40 60 80 100 120

Fig. 13. Synthesis of (a) probability ratios and (b) intensity changes when comparing the return period and magnitudes of the 2023 annual 2-day maximum rainfall, area-averaged over the study region in the current climate and a 1.2°C cooler climate.

(a) Probability ratio

0.01 0.1 1 10

AM2.5C360 amipHistorical+rcp4.5SST (3)

FLOR historical-rcp4.5 (10)

HadGEM2-ES r1 CCLM5-0-15 hist-rcp8.5 (1)

HadGEM2-ES r1 RegCM4-7 hist-rcp8.5 (1)

HadGEM2-ES r1 REMO2015 hist-rcp8.5 (1)

MPI-ESM-LR r1 CCLM5-0-15 hist-rcp8.5 (1)

MPI-ESM-LR r1 REMO2015 hist-rcp8.5 (1)

MPI-ESM-MR r1 RegCM4-7 hist-rcp8.5 (1)

NorESM1-M r1 CCLM5-0-15 hist-rcp8.5 (1)

NorESM1-M r1 RegCM4-7 hist-rcp8.5 (1)

NorESM1-M r1 REMO2015 hist-rcp8.5 (1)

models

(b) Change in intensity

-30 -20 -10 0 10 20 30 40

**Fig. 14** As Fig. 13, but for models only of a 0.8°C warmer (2°C since pre-industrial) climate.

7 Vulnerability, exposure, and resilience

Focusing solely on the hazard, the cyclone, only tells one part of the story about the impacts experienced in this region. By exploring its interaction with the additional disaster risk factors, this section discusses the key exposure, vulnerability, and coping capacity factors, as well as additional natural and social shocks, which influenced the likelihood and severity of impacts from the heavy rainfall event. Vulnerability indicates a person, community, system, or asset's propensity to be impacted by a hazard

2 l

(see e.g. Kelman *et al.*, 2016), while exposure entails the degree to which people, systems, or assets are located in a hazard-prone location (UN-SPIDER, n.d.).

Much of the impacts from the Cyclone Gabrielle-associated floods, conceptually illustrated in Figure 15, occurred in Te Matau-a-Māui and Te Tairāwhiti. Communities across Te Tai Tokerau, Te Tara-O-Te-Ika-A-Māui, and Tāmaki Makaurau regions are also severely impacted (MetService, 2023a; Beehive.govt.nz, 2023). It is important to examine this event through the lens of compound events (Zscheischler *et al.*, 2018) and understand the antecedent conditions, both from a hazard perspective and a social one (Thalheimer *et al.*, 2022). For example, Cyclone Gabrielle was preceded by Cyclone Hale which also led to severe flooding, and it hit during a time when Aotearoa is facing a severe cost-of-living crisis notably driven by the COVID-19 pandemic and labour shortages (Te Putea Matua/Reserve Bank of New Zealand, 2022a). Annual inflation in Aotearoa reached 7.2 percent in 2022, a three-decade high implying that those already economically disadvantaged will have a harder time re-building (Te Putea Matua/Reserve Bank of New Zealand, 2022b). Further, the impacts also cascaded across multiple sectors (Figure 15). For example, the flooding damaged electrical infrastructure, which led to power outages, and made it harder for people who depend on cashless payments to buy things (Strait Times, 2023).

The section will examine social vulnerability, land-use change and infrastructure, and risk management policies and systems in order to offer context on key facets of vulnerability and exposure that mediated the impact of the extreme rainfall from Cyclone Gabrielle, and may be used to inform adaptation planning and recovery after the event.
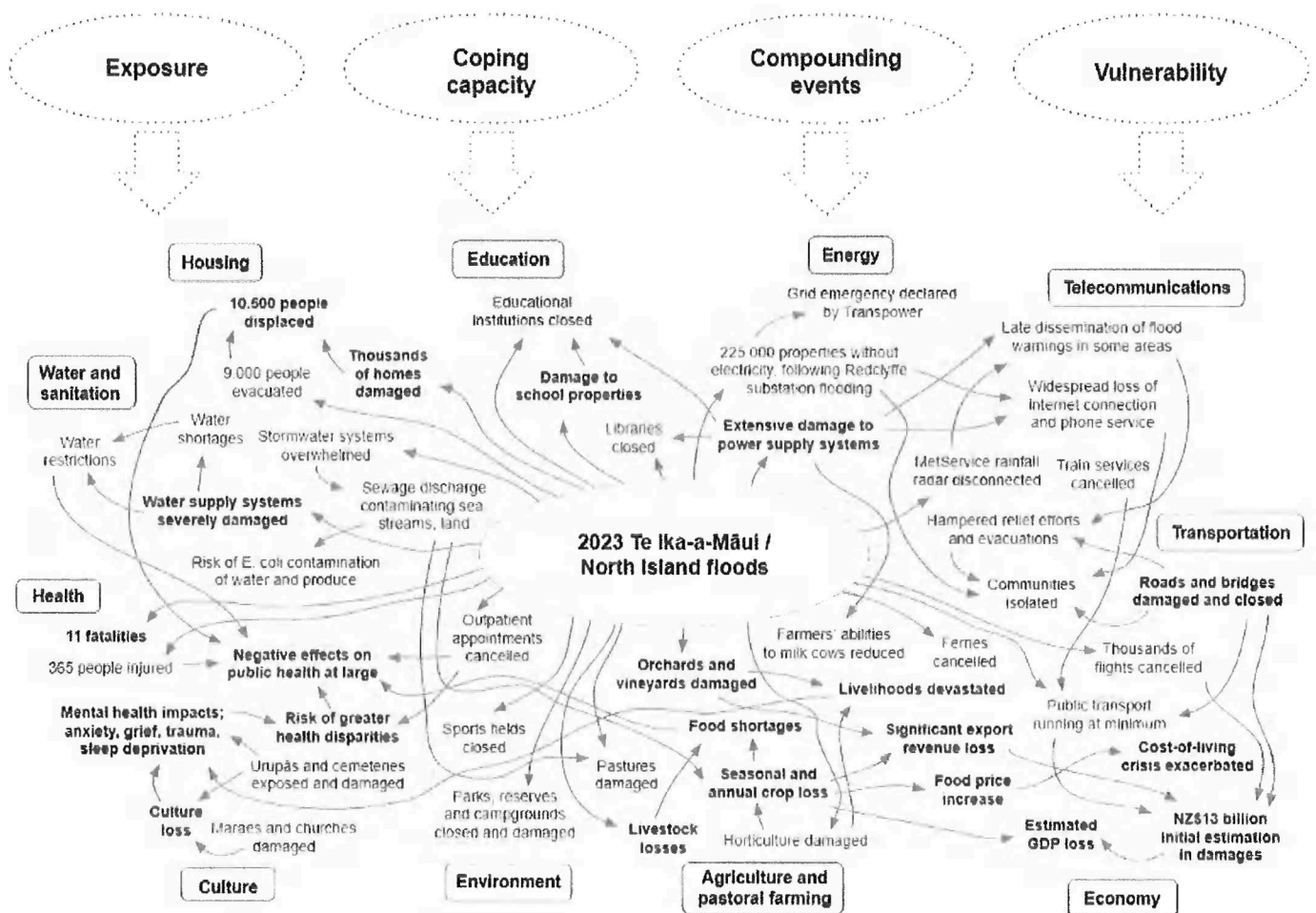
Figure 15. Impacts pathways among sectors affected by the 2023 Te Ika-a-Māui floods. Exposure, vulnerability, coping capacity and compounding events make out the context in which the flooding occurred and shape the disaster risk along with the main hazard subject to the study's attribution analysis. Long-term impacts are emphasised in bold.

7.1 Social vulnerability

To bridge a critical gap in understanding of flood vulnerability in Aotearoa, the country's most frequent and damaging hazard, Mason et al. (2021) identified 10 dimensions of social vulnerability to flooding. Social vulnerability entails people and communities' susceptibility to adverse impacts of a natural hazard such as flooding (Raduszynski and Numada, 2023). These ten social vulnerability dimensions are discussed in the context of prevalence across the flood-affected regions.

Risk knowledge, skills, and awareness are fundamental to risk judgement and in turn managing the threat that flooding poses. Trust in authorities and repeated risk communication are both linked to greater flood risk perception (Maidl and Buchecker, 2015; Samaddar *et al.*, 2012). Past experience with flooding is an important indicator of greater risk perception (Mondino et al., 2020), which is known to have enabled more timely response among communities in Te Tai Tokerau (Auliagisni, Wilkinson and Elkharboutly, 2022) and Te Tairāwhiti (Warmenhoven *et al.*, 2014). Those without previous experience, on the other hand, are more inclined to disregard flood warnings and defy voluntary evacuation instructions (Auliagisni, Wilkinson and Elkharboutly, 2022). The lack of comparable events, or few and far in between, may have negatively influenced people's ability to assess the risk they were

facing. Households without reliable access to telecommunications such as the internet and phones, people new to the area or country, and people with limited English proficiency usually display lower risk awareness (Mason *et al.*, 2021). Compared to the national average, all flood-affected regions indicate higher vulnerability in terms of access to telecommunications (see table 4).

Dependence on care support is another factor which affects a person's risk awareness as well as the ability to manage the risks (Mason *et al.*, 2021; Rufat *et al.*, 2015). People of young (<15 years) and old (>65 years) age, as well as people living with disability or other pre-existing health conditions are disproportionately vulnerable (Kuhlicke *et al.*, 2011; Bigi *et al.*, 2021). These health conditions include mobility, vision, hearing, learning, or intellectual impairment, to mental illness, cardiovascular or respiratory disease, pregnancy, and people reliant on medication or health services for their wellbeing (Mason *et al.*, 2021). Aotearoa's 2013 Disability Survey demonstrated that nearly one-fourth of the population identify as disabled, as in limited in their daily activities, with the highest rates among elderly and Māori populations (Rapu Matauranga Hauora mo te Taiao - Aotearoa, 2014).

Additional factors key to the management of flood risk include ability to financially cope with crisis and losses, as well as enough food, water and other basic necessities to cope with societal disruptions to supply chains and potential shortages (Mason *et al.*, 2021; Paterson, Wright and Harris, 2018; Alderman, Turner and Tong, 2012). Unemployment, low educational level, households without access to a car, socioeconomic deprivation, and single parent households are indicators of structural vulnerabilities. There are significant economic disparities between Māori and non-Māori populations, with the former suffering nearly twice the unemployment rate of the national average (see Table 4), and a median income lower than all other ethnic groups in the country (Hikina Whakatuki, 2021). Te Tairawhiti, one of the most severely affected regions, is home to the country's largest Maori population as well as the highest deprivation levels (Te Whatu Ora/Health New Zealand, 2019).

A high degree of social connectedness can help offset socioeconomic vulnerability to some extent by increasing adaptive capacity, as social capital in the forms of networks, neighbourhood cohesion, and trust can enable community members to act towards shared objectives and help each other overcome hurdles (Bixler *et al.*, 2021). There are multiple anecdotal examples of this (see e.g. Stuff, 2023; NZ Herald, 2023). Notably, communities in the Waiapu catchment of Te Tairāwhiti have strong social capital in the form of kinship networks that contribute to strong social cohesion (Warmenhoven *et al.*, 2014). People new to the neighbourhood or country, single parent or single person households, and elderly populations tend to have smaller social networks (Walkling and Haworth, 2020; Mason *et al.*, 2021; Wethington, Pillemer and Principi, 2016). A high degree of participation and inclusion in decision-making is moreover considered a resilience strengthening factor, in part because it increases the likelihood that all perspectives and needs are adequately accounted for (Feteke *et al.*, 2021; Burningham, Fielding and Thrush, 2007).

For vulnerabilities to lead to impacts, people, systems or assets must be exposed to the given hazard (Simpson *et al.*, 2014). Indicators for exposure in Aotearoa range from number of people and households in the affected area (direct exposure), and people commuting outside of the flood-affected area and live in remote or rural communities (indirect exposure), to workers in health care, as first responders, or in the primary industries of farming and forestry (occupational exposure) (Mason *et al.*, 2021). Settlements and infrastructure on the coast, by rivers, and near hills are particularly exposed to floods (Auliagisni, Wilkinson and Elkharboutly, 2022). Safe, secure, and healthy housing is key to ensuring that individuals and communities can withstand the exposure to flooding. Crowded households, also associated with higher vulnerability, are more prevalent among families of Māori and

2.4

Pacific descent (Pearson, 2018). These ethnic groups more often reside in housing of inferior standard compared to the national majority (Pearson, 2018). Rural Māori communities across Te Tai Tokerau, Te Tairāwhiti, Te Matau a Māui, and Hauraki regions are among the most impacted, subsequently struggling to secure shelter following significant damage to homes while isolated due to damage to roads, bridges, and telecommunications (NZ Herald, 2023b).

Māori populations are disproportionately vulnerable and exposed to hazards such as the studied floods, as political, economic, social, and cultural marginalisation has been entrenched through the British colonisation of Aotearoa (Hobbs et al., 2019). Meanwhile, it is also important to note that most social vulnerability data referenced in this section was collected via the 2018 Census and may be slightly out of date given the significant economic and social shifts since then.

Table 4. Prevalence of social vulnerability indicators across the national and flood-affected regions' populations, with values disaggregated between total regional population (RT) and regional Māori population (RM). Values for flood-affected regions are colour coded to illustrate how they compare to the national total population average (NT), where green equals lower prevalence and red equals higher prevalence. National Māori (NM) prevalence averages are included for reference. The data is collated through the 2018 Census (Statistics NZ, 2018a, 2018b, 2018c, 2018d, 2018e, 2018f).

Social vulnerability indicator	National prevalence (% of population)		Regional prevalence (% of population)									
	NT	NM	Te Matau-a-Māui		Te Tairāwhiti		Te Tai Tokerau		Te Tara-O-Te-Ika-A-Māui		Tāmaki Makaurau	
			RT	RM	RT	RM	RT	RM	RT	RM	RT	RM
Children (<15 years)	19.6	31.65	21	32.95	23.7	30.85	21.25	32.1	14.3	30.1	20	31.85
Elderly (>65 years)	15.2	6.1	18.3	7	15.5	8.35	19.55	8.35	29.25	10.3	12.1	4.95
Unemployment	4	8.1	3.6	7	5.2	7.9	5.2	10	2.6	4.1	4.1	7.9
No educational qualification	18.2	25.3	22.6	27.8	23.8	27	23.1	28.2	26.4	26.6	14.5	24
Not in the labour force	31.1	29.4	32.8	30.3	32.7	32.5	37.1	34.4	43.2	32.8	30.4	28.9
Residence elsewhere in ANZ 1 year ago	16.7	19.5	15.2	17.5	15.3	16.6	16.8	18.7	17.6	23.9	15.6	18.4
Arrival to country <1 year ago	5.9	N/A	6.2	N/A	4.9	N/A	4	N/A	2.2	N/A	5.5	N/A
Households without access to telecommunications	1.1	N/A	1.3	N/A	2	N/A	1.5	N/A	1.4	N/A	1.2	N/A
Households without access to basic	0.4	N/A	0.3	N/A	0.3	N/A	0.3	N/A	0.5	N/A	0.6	N/A

amenities											
Housing not owned	35.5	N/A	33.	N/A	40.6	N/A	32.1	N/A	29.7	N/A	40.6	N/A

In a recent government report, 44 communities across Aotearoa were identified to be facing high flood risk, based on socioeconomic vulnerability, flood exposure, lack of plans to build flood protection infrastructure, and limited financial capacity among the wider district to fund flood risk responses (Te Tari Taiwhenua, 2022; Rapu Matauranga Hauora mo te Taiao - Aotearoa, n.d.). Over half of these high risk communities are located in the top half of Te Ika-a-Māui, with clusters of high risk communities in Te Tai Tokerau, Te Moana-a-Toi, Te Tairāwhiti, and Waikato. All of these areas have significantly high populations of Māori (Statistics NZ, 2022). Some of these high-risk regions are consistent with the most affected areas in the 2023 Te Ika-a-Māui floods.

7.2 Land-use change and infrastructure

7.2.1 Land use change

Some of the worst affected areas from this extreme rainfall event were in urban centres along Te Matau-a-Māui, including Heretaunga (Hastings) and Ahuriri, which have many areas of built infrastructure (flood protection systems) along river floodplains. The flood systems, such as those along the Heretaunga Plains and Ruataniwha Plains, are able to withstand "regular" floods from storms that affect the Bay on an annual to decadal basis; however, high-intensity events such as this one are often able to overwhelm flood defences for the built environment, which are generally built to the standard of a 1% Annual Exceedance Probability (AEP) (Te Kaunihera A-Rohe o te Matau-a-Maui, 2020).

The regions affected by the extreme rain event were also exposed to increased vulnerability as, post European settlements, the converted hills (from forestry to pasture lands) reduced the strength and stability of soils, making these areas more susceptible to landslides (Glade, 2002). Post European settlements, the removal of stabilising vegetation along the river beds also increased soil erosion, which further increased the region's vulnerability to landslips and slides (Wilmhurst, 1997). Additionally, forest clearance and management practices along steep terrains within the region have increased debris flows and landslide materials into river systems (Brierley et al., 2022). The European colonisation of the indigenous lands has not only led to increased flood risk from poor land use management, but also a multitude of Indigenous environmental injustices such as the draining of wetlands and remaking of waterscapes to align with utilitarian Pākehā (European) values (Parson & Fisher, 2022; Brierley et al., 2022).

The floods significantly affected the northern, rural communities of the Te Tai Tokerau and Te Tairāwhiti regions. The economy of these less urbanised areas are based on agriculture, fishing, forestry, and horticulture. These small communities (e.g. Hauraki, Te Tairāwhiti, Wairoa, and Te Tai Tokerau) have inherent vulnerabilities as they are mainly accessible by a single roading network, which often run through short river catchments with steep topography most damaged by extreme flooding. For example, Māori communities in Te Tai Tokerau, Te Tairāwhiti, and Hauraki were left without adequate resources for more than ten days after the storm, some of which were entirely unreachable due to infrastructure damage from flooding (NZ Herald, 2023c). Tokomaru Bay in Te Tairāwhiti is still cut off from north and south, only accessible by sea or air (RNZ, 2023-c).

7.2.2 Energy infrastructure

The existing centralised energy infrastructure within Aotearoa also contributed to enhanced vulnerabilities from the flood event. The power outages and impacts from the floods were exacerbated due to outages from single point energy system failure (Stuff, 2023b). At the height of this disaster's impacts, over 225,000 homes across the Te Ika-a-Māui were without power, including over 45,000 in Te Matau-a-Māui alone (Stuff, 2023c). To repair the exposed power grid's electricity lines network, costs will likely total approximately NZ$100 million, making this extreme event the largest impact to the power system since Cyclone Bola in 1988 (Newsroom, 2023; The Guardian, 2023b).

7.2.3 Deforestation: forestry slash

Similar to the European colonial alterations to hillsides in Te Ika-a-Māui, deforestation also significantly disrupts the land's natural resilience to extreme rainfall events (Stuff, 2023d; Gholoubi *et al.*, 2019). Forestry slashing has become a significant issue within the region (Stuff, 2023e, Charlton, 2021). Forestry "slash" is a waste product from commercial forestry, ranging from small branches to whole trees and other debris that are left behind, and stay behind for years, after wood is harvested (Stuff, 2023f, Wagenbrenner *et al.*, 2016). The slash often creates dams along the rivers when flooding increases the flow of the debris including trees, mud, and silt. These forest slash impacts were felt after Cyclone Gabrielle with mud and debris flowing in several already vulnerable areas such as Te Tairāwhiti and Te Matau-a-Māui, with significant impacts along the road between Wairoa and Te Tairāwhiti (The Guardian, 2023c). A notable example of slash affecting already vulnerable populations was the complete destruction of the major bridge along the East Coast SH35 highway connecting Tolaga Bay and Tokomaru Bay (RNZ, 2023b).

7.3 Risk management

Risk management practices and policies are a key to mitigate disaster impacts and can be conceptualised here through at least four phases of the disaster risk management continuum.

Cyclone Gabrielle and its subsequent flooding was particularly well-forecasted and communicated. The cyclone was monitored from as early as 10 days before and was forecasted to hit New Zealand approximately with a lead time of approximately 7 days (MetService, 2023b). From this, Aotearoa's national early warning system has recently undergone revisions and these improvements have been well-noted (Stuff, 2021; Stuart-Black, 2021) - the country also has an automatic warning system that disseminates emergency alerts (I Te Wa Ohotata, n.d.). The weather warnings were widely available on weather and news channels. Based on this, emergency management agencies instructed the public to stock-pile three days worth of food, water and supplies (Stuff, 2023g). Mandatory evacuations were undertaken for at least 9.000 people across Te Matau-a-Māui (Stuff, 2023h; NZ Herald, 2023c) and 50 apartments in the Tāmaki Makaurau region (NZ Herald, 2023d). In addition, many civil society organisations and municipal councils communicated warning information to their citizens, for example Māori radio station's contributed to disseminated official information from the GDC and Te Tairāwhiti Civil Defence and local marae opened their doors to those in need (The Spinoff, 2023b). The New Zealand Red Cross (n.d) also has its own weather warning app. During the event,however, the MetServices's radar was disconnected mid-event, and combined with telecommunication and energy breaks this meant that the regional council in Te Matau-a-Māui was left unable to access and transmit information (MetService, 2023a; MetService, 2023b).

If, at first glance, the early warning system therefore seems to have worked as it should have and with a relatively good lead time, many wonder why the impacts were so significant. Various theories can be posited here and will certainly be the subject of more in-depth study. For example, did communities experience warning fatigue/disengagement? Was the magnitude of the flooding misunderstood by emergency managers and local communities alike? Did the timing of the peak rainfall play a role, having arrived in the middle of the night (such as for the particularly devastated Esk Valley)? What were the contingency and early action plans followed by emergency managers, telecommunications companies, road maintenance crews and other essential services? Or simply, could it be said that this was an extreme event with relatively low morbidity and mortality, and in this case the warnings must have worked in this essential way? An after-action review exploring these questions will be essential to improve early warning and early action systems going forward.

Many affected communities are currently entering the recovery phase which will determine how quickly they can bounce back from the event. This has been coordinated at municipal and national level, with mayoral relief funds set up for the most affected regions (I Te Wa o Ahuriri, 2023), Red Cross appeals (Stuff, 2023i), tribal kinship networks (Waatea, 2023), and various pledges from the national government for activities such as road repavement (a NZ$250 million package) (Beehive.govt.nz, 2023b), immediate local business relief (NZ$50 million package) (New Zealand Government, 2023), and Maori led responses (Te Puni Kōkiri, 2023). Finally, Aotearoa has very high private insurance coverage and insurance companies which are used to dealing with major events (Te Kahui Inihua o Aotearoa, n.d), both of which increase recovery speed which is essential to decreasing the long-term impacts of a disaster like this one. It is estimated that Cyclone Gabrielle will have cost insurers over $1billion with over 47.000 claims already made on March 6th (RNZ, 2023c). On that date, over $111 million had been paid, leaving many people still waiting (RNZ, 2023c).

For some places and people, recovery may no longer be a feasible option. Even before the floods resulting from Cyclone Gabrielle, the government was developing a system for managed retreat in Aotearoa, with plans to introduce legislation by the end of 2023 in order to address legal and funding issues (Manatu Mo Te Taiao, 2022). Managed retreat is also central to Aotearoa's National Adaptation Plan (NAP, 2022). Managed retreat is seen as a last resort, when other adaptation options like building sea walls, or raising properties are no longer feasible (NAP, 2022). This option presents particular challenges for Māori communities who may want to maintain connection with sites of cultural importance, and have a unique spiritual connection to the land and natural resources (Manatu Mo Te Taiao, 2022).

There is growing recognition amongst decision-makers that Māori, particularly tribal representatives, ought to be involved as co-governance partners in natural resource management (Maxwell et al., 2020) and disaster risk reduction approaches (Kenney, 2019). Many policymakers are also willing to incorporate Māori perspectives and knowledge into disaster risk reduction approaches in Aotearoa (Kenney, 2019; Lambert and Mark-Shadbold, 2021). However, the implementation of policy responsive to Mātauranga Maori to date has been imperfect.

7.4 V&E Conclusions

Aotearoa is a country with good channels for communicating forecasts of extreme rainfall. Significant warning was able to be given for Cyclone Gabrielle of expected heavy rainfall and the potential for rapidly rising rivers, which may have reduced impacts. Still, the significant damage, economic cost,

and loss of life can be linked to factors such as a reliance on flood protection systems and infrastructure that are not built to withstand such extreme flood events, settlements in highly flood-prone regions, and social vulnerability factors that can reduce coping capacity such as higher rates of disability and unemployment amongst Māori communities. Land use changes that reduced soil stability, combined with deforestation and forestry slashing likely also contributed to the impacts. Future efforts to reduce vulnerability should focus on addressing shortcomings such as updating infrastructure to be built to the "new normal", and strengthening early-warning systems for impacts, social connectedness, knowledge, skills and awareness of natural hazards which can improve risk perception and increase self-protective action based on a forecast or warning. Adaptation efforts must be inclusive of a variety of stakeholder viewpoints, especially Indigenous cultural values that may differ from Pākehā views of flood risk management (Parsons and Fisher, 2022).

Acknowledgements

Data availability

Almost all data are available via the Climate Explorer. For data not available on the Climate explorer please contact Sam Dean at NIWA.

Appendix

Location-specific return period estimates

While most of our analysis has focused on annual two-day maxima of rainfall data which was first averaged across the whole Te Matau-a-Māui and Te Tairāwhiti regions - for the reasons explained in Section 1.4 - there of course needs to be further consideration of how the relative intensity of rainfall associated with Cyclone Gabrielle varied for individual locations within the region. This additional context is important, since a return period of any value for the region as a whole will be made up of a range of different local experiences. As an example of this, Figure S1 presents preliminary estimates of return periods for two-day rainfall accumulations associated with Cyclone Gabrielle across Te Matau-a-Māui. While uncertainty estimates around these numbers will be necessarily large, particularly for those stations with shorter record lengths, it is evident that geographic diversity exists when considering the relative rarity of the rain which fell across different parts of the region. For those places most heavily impacted, best-guess return period estimates range from a 1-in-70 through to a 1-in-320 year event, while other stations saw rainfall amounts more consistent with a 20-year return period or less.

This emphasises the importance of understanding how to interpret any return period estimate when talking about extreme rainfall across a widespread region: if Cyclone Gabrielle was consistent with a 1-in-30 year event across the entire Te Matau-a-Māui and Te Tairāwhiti region, this does not mean that

the amount of rain which fell in every individual location therein experienced rainfall was also consistent with a local 1-in-30 year event.

Gabrielle Rainfall
48 hour duration return period

Return Period (years)
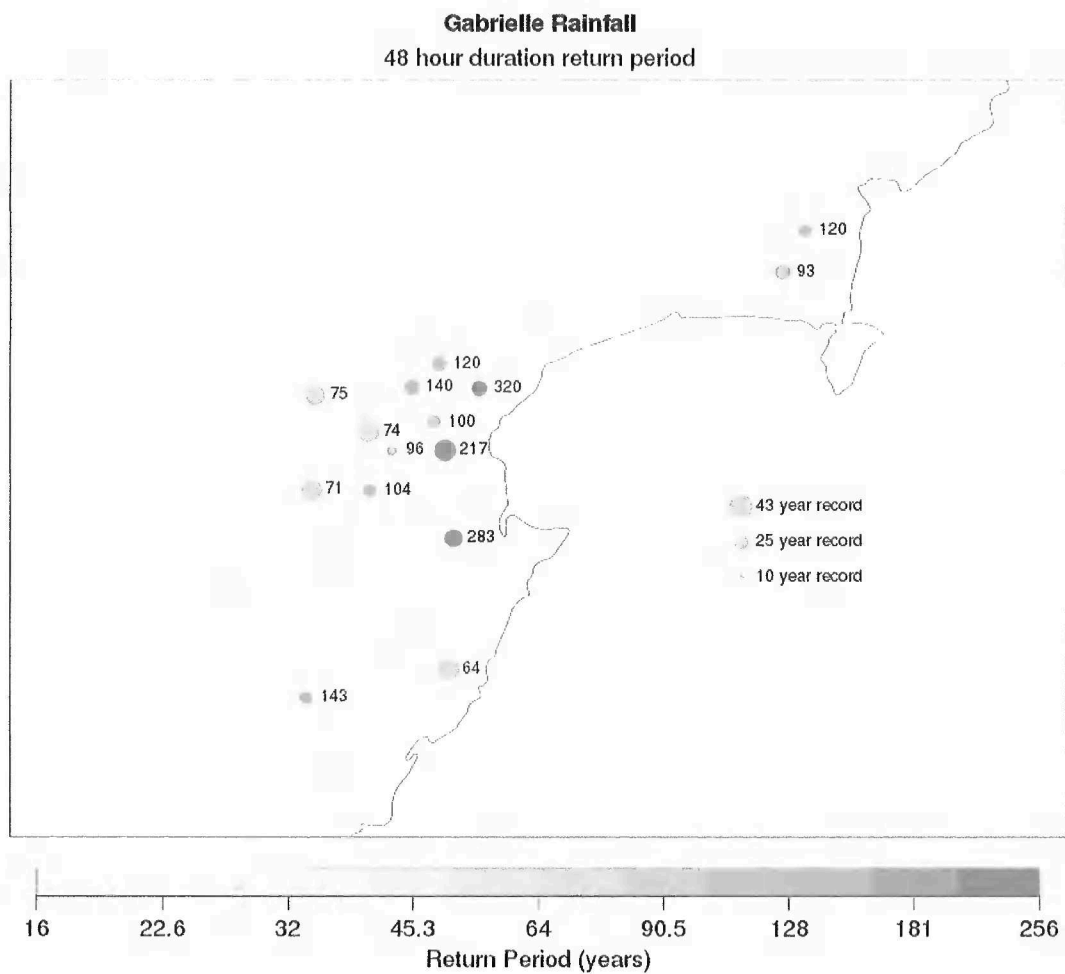
Figure S1: 48-hour return period estimates for individual rainfall stations (including available regional council gauges, NIWA and MetService station data) across Te Matau-a-Māui region. Figure credit: Trevor Carey-Smith (NIWA).

It's also worth reiterating that experiencing an event with a "1-in-20-year return period" does not mean that a similarly impactful event will then not occur for another 19 years. Rather, this means that an event of at least that magnitude has a 5% chance of occurring each year (5% being 1/20th of 100%). Figure S2 demonstrates this variation in the potential to experience a 1-in-N year event well before N years of additional observations occur (with this example assuming non-stationarity): for example, there is approximately a 1-in-3 chance of experiencing a 1-in-50 year event within twenty years.
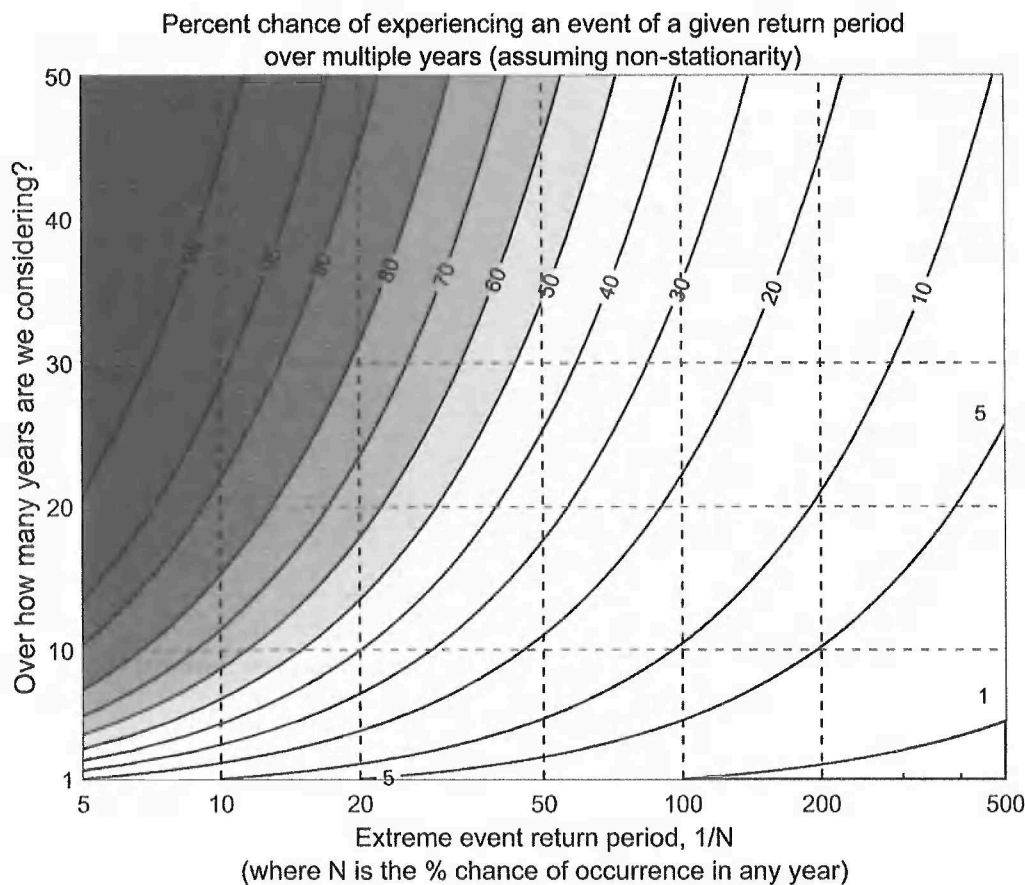
Figure S2: Schematic demonstration of how to interpret the probability of experiencing an event, described as a 1-in-N year return period, over subsequent years (assuming non-stationarity in this example).

Sensitivity of results to differences across observational products

As discussed in further detail in Section 3.2, differences exist between the two observational products with respect to the relative rarity of the rain which fell during Cyclone Gabrielle - this likely relates to the fact that not all available observations would have been immediately integrated into MSWEP's representation of the event, owing particularly to breakdowns in some station reporting in the days immediately following the event. However, aside from this discrepancy, there remains otherwise good agreement on the relative magnitude of Rx2day in other years when comparing MSWEP with the 11-station observational product (see figure S3). Both show clear peaks in previously known extreme events, including Cyclone Bola (1988), aalthough the composite product shows a slight decreasing trend, while MSWEP shows an increasing tren. For reference, the subsequent GEV analyses - comparable to the results shown in Section 3.2 - are also presented for each of the two observational products side-by-side in Figures S4 and S5.

rx2day in MSWEP & station composite
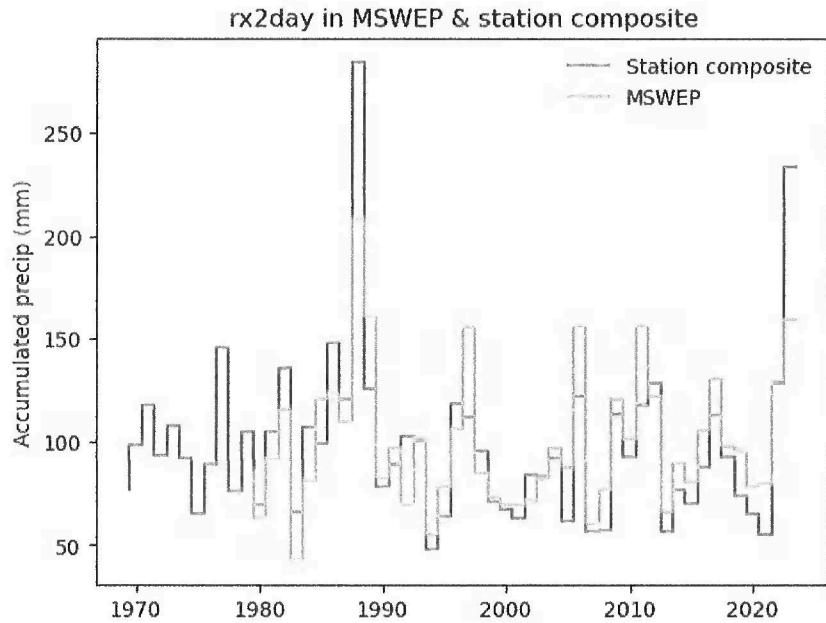
Figure S3: Time-series of Rx2day for the analysis region, for MSWEP (orange lines) and the 11-station observation product (blue lines).
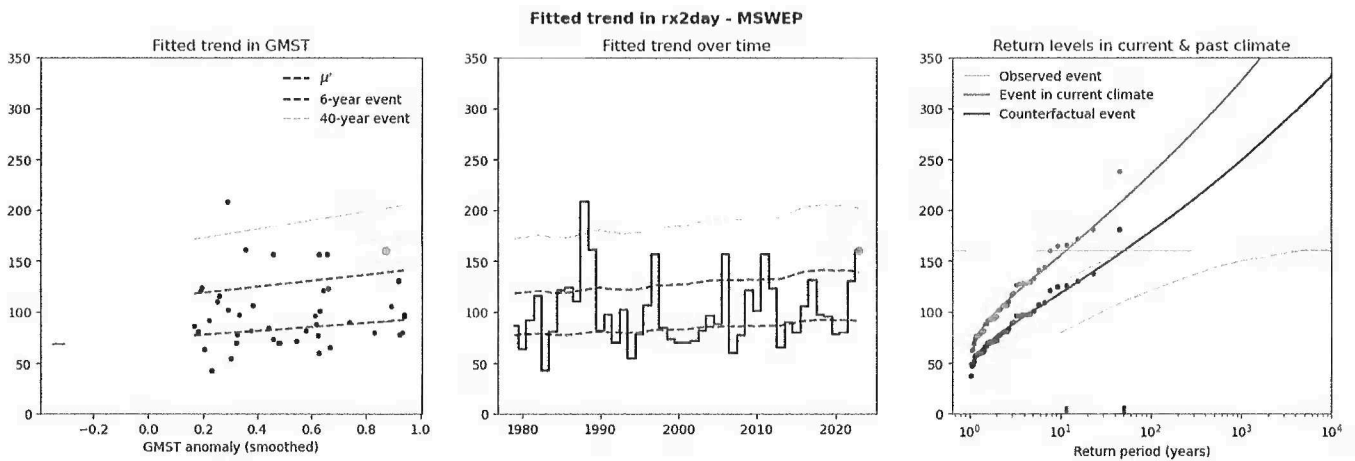
Figure S4: GEV trend analysis for the MSWEP observational product (similar to the results shown in Section 3.2)
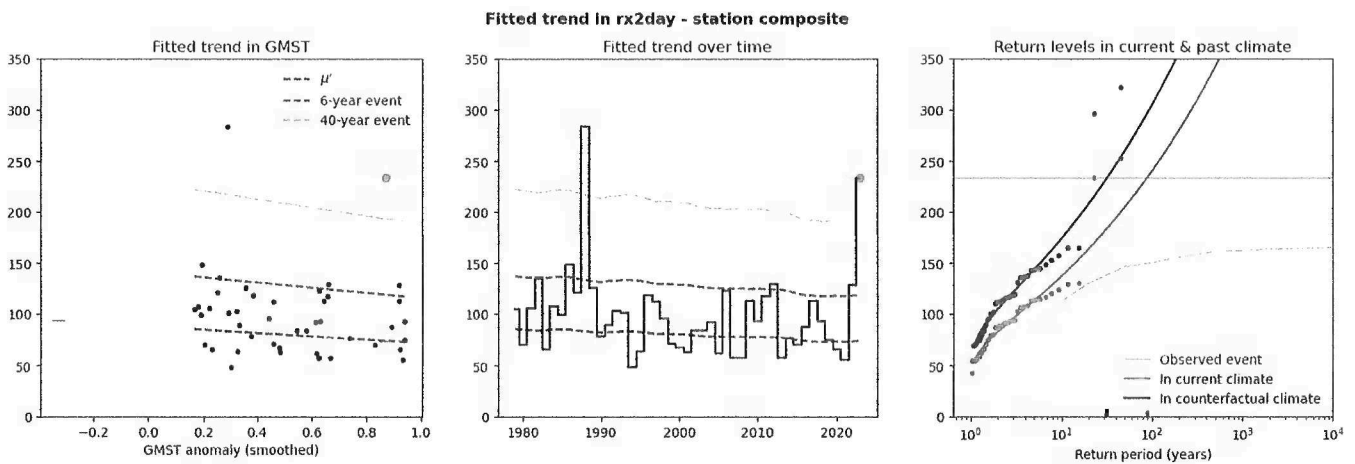

**Figure S5: Same as Figure S4 but showing the GEV trend analysis for the 11-station observational product.**

Spatial characteristics of extreme rainfall in climate models

One aspect of the model evaluation process involves examining the spatial characteristics of climatological mean Rx2d for each of the models, relative to those of the historical climatology of MSWEP (figure S6). An example of some of the models which passed this test are shown below for the nine CORDEX models (figure S7)
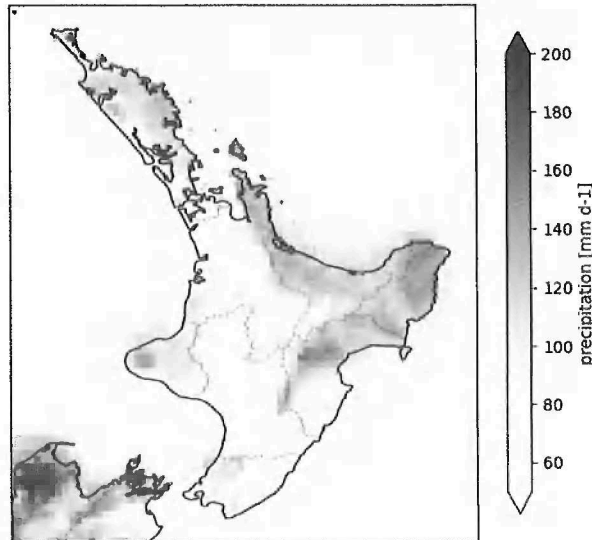
Figure S6: Climatological mean Rx2day for all grid cells from MSWEP (using data from 1979-2022).
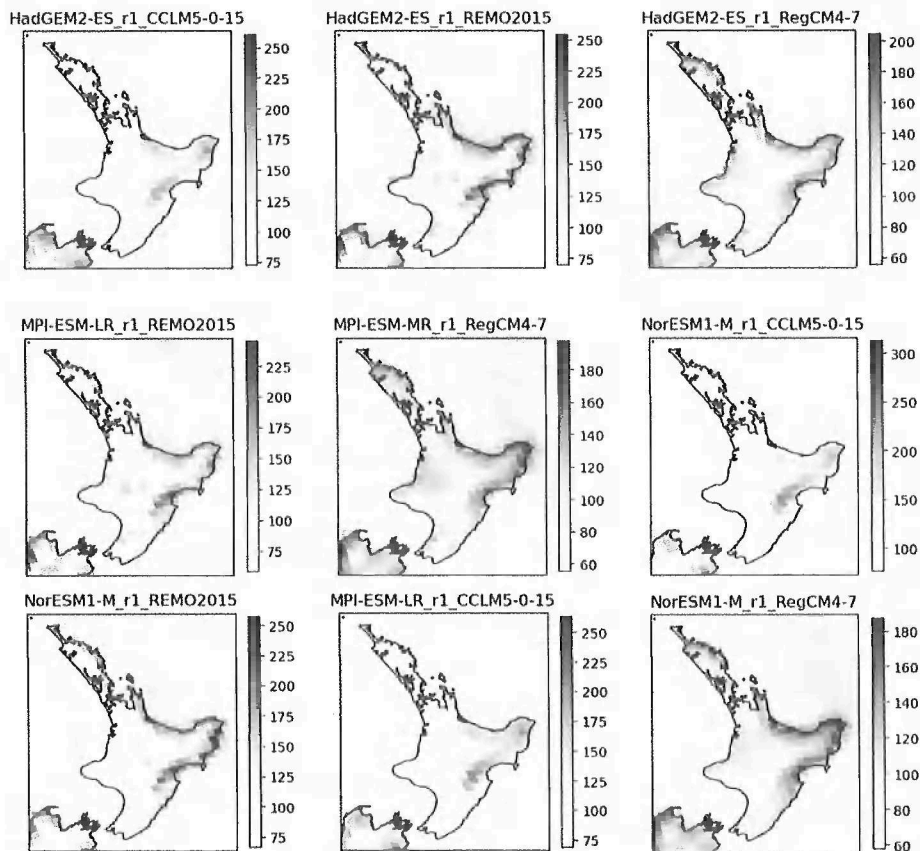
Figure S7: Corresponding representations of Rx2day climatologies in each of the nine CORDEX models which passed the evaluation criteria.

33

Comparing best-guess estimates of changing event frequency and intensity across different models

Across the range of climate models examined in Section 5, clear differences have emerged in the best-guess estimates of changing frequency and intensity of extreme rainfall like the rain associated with Cyclone Gabrielle, due to 1.2°C of global temperature rise. However, as revealed in Figure S8, a clear relationship does emerge when comparing each model's best-estimated change in the intensity of the event and the corresponding best-estimate of change in the frequency of the event. For example, those models which exhibited a best-guess 5-10% intensification of rainfall from an event similarly rare to Cyclone Gabrielle also found between a 50% increase and doubling in the frequency of such events.
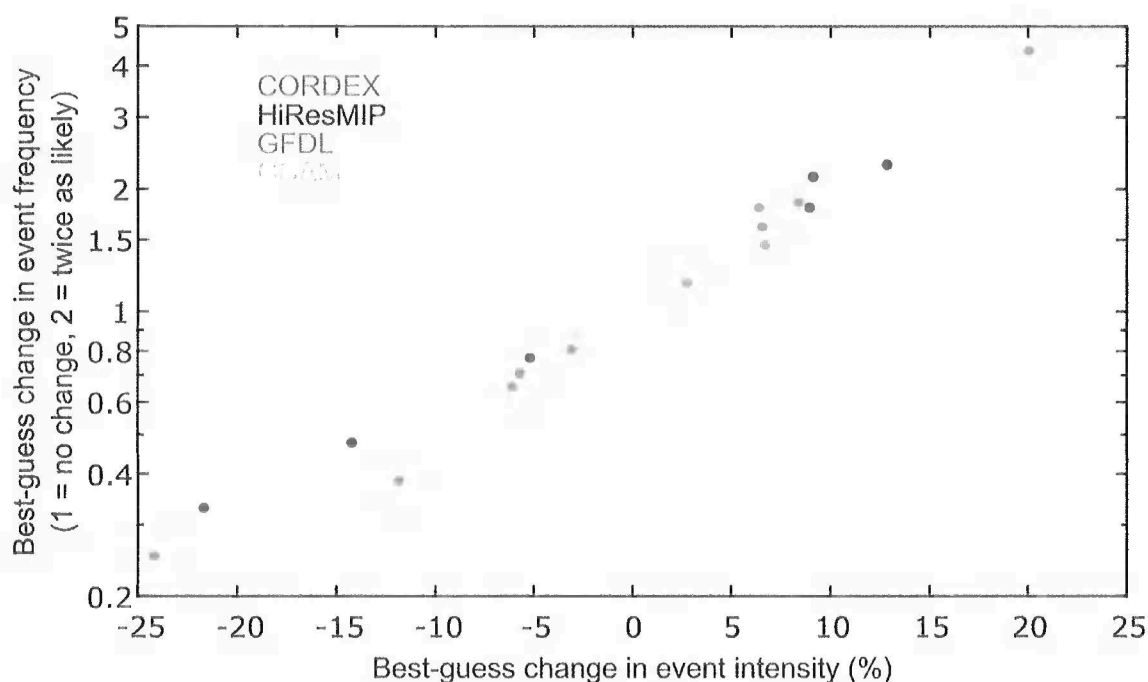
Figure S8: Comparison of modelled best-guess estimates in the intensity of Cyclone Gabrielle-like rainfall event (x-axis), and the corresponding best-estimated change in frequency of such events between the current climate and a 1.2°C- cooler climate (y-axis).

Topography of Te Ika-a-Māui

The topography of Te Ika-a-Māui is a critical point of reference when understanding the spatial characteristics of extreme rainfall within both climate models and the observational data used. This information is presented in Figure S9.
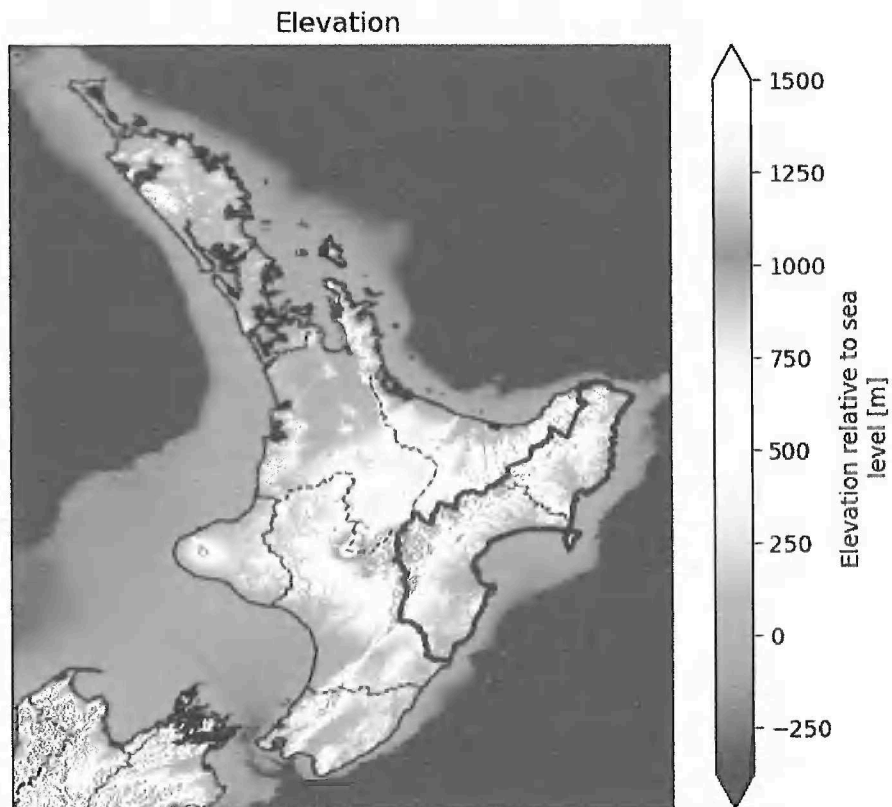
Figure S9: Elevation profile for Te Ika-a-Māui. The red outlined region indicates the analysis region for this study